의학박사 학위논문

The Role of SENP2 in Metabolism of Brown Adipose Tissue

갈색지방조직에서 SENP2의 대사적 역할 규명

February 2023

서울대학교 대학원
내과학

최 훈 지

The Role of SENP2 in Metabolism of Brown Adipose Tissue

Hun Jee Choe

Submitting a Ph.D. Dissertation of Medicine

October 2022

Graduate School of
Seoul National University
Internal Medicine Major

Confirming the Ph.D. Dissertation

January 2023

Chair _____(Seal)
Vice Chair _____(Seal)
Examiner _____(Seal)
Examiner _____(Seal)
Examiner _____(Seal)

Abstract

Brown adipose tissue (BAT) is a metabolically active endocrine organ. Activation of BAT contributes to increased energy expenditure through systemic glucose and lipid utilization. SENP2 is a post-translational protein modifier that is involved in regulation of metabolism in different tissues. How SENP2 may modulate BAT activity has not been elucidated yet.

Here, I demonstrate that SENP2 is involved in effective adaptive thermogenesis by increasing the transcriptional activity of UCP1. BAT-specific *Senp2* knockout (*Senp2*-BKO, *Ucp1*-Cre;*Senp2*$^{f/f}$) mice showed normal adipogenesis and growth. These mice were, however, intolerant to acute cold exposure and were more insulin resistant in response to high fat diet than controls. Mechanistically, knockdown of *Senp2* in brown adipocytes resulted in reduced levels of *Ucp1* and *Cidea* through SUMOylation of PGC-1α and ERRα. Specifically, deSUMOylation of ERRα enhanced the synergistic effect of ERRα/PGC-1α complex.

Collectively, these results suggest that SENP2 is intimately involved in modulating the activity of BAT through deSUMOylation of ERRα/PGC-1α complex, especially ERRα. Activation of BAT through SENP2 may be a potential therapeutic target in ameliorating metabolic stress.

Keyword: Brown adipose tissue, SENP2, metabolism, UCP1, ERRα, PGC-1α
Student Number: 2019-38931

Table of Contents

List of Table and Figures

Chapter 1.
The Role of SENP2 in Brown Adipose Tissue

1. Introduction

Recently, brown adipose tissue (BAT), a thermogenic fat that dissipate energy as heat, has garnered much attention as a therapeutic target for metabolic diseases [1, 2]. Ample evidence that supports the presence of metabolically active BAT in adult humans have generated enthusiasm [3-8], as activated BAT not only contributes to non-shivering thermogenesis (NST), but also increases energy expenditure by increasing the utilization of free fatty acids and glucose. In a retrospective study that reviewed 52,487 patients with or without detected BAT activity on ^{18}F-FDG positron emission tomography-computed tomography scans, propensity score matched analysis revealed lower prevalence of cardiometabolic diseases in individuals with active BAT [9].

SUMO (small ubiquitin-related modifier) is a reversible post-translational protein modifier [10-12]. The exquisiteness of this enzyme comes from the enigmatic consequence of SUMOylation and deSUMOylation. SUMOylation process closely resembles ubiquitylation in that it requires an enzymatic cascade that involves activation of a mature SUMO protein, conjugation, and transfer which is catalyzed by E3 ligases [13]. While ubiquitylation typically results in degradation, SUMOylation may induce alteration in cellular localization, activity, or stability of proteins depending on the target. SUMO proteins can be deSUMOylated by SUMO-specific proteases (SENPs) – namely, SENP1, 2, 3, 5, 6, and 7 in mammals – with different substrate species and cellular location.

Of these, SENP2 undertakes eminent metabolic roles in different organs. In skeletal muscle, SENP2 increases fatty acid oxidation (FAO) via deSUMOylation of peroxisome proliferator activated receptor (PPAR) proteins. By recruiting deSUMOylated

PPARδ and PPARγ to the promoters of FAO associated enzymes i.e., carnitine palmitoyl transferase-1 (CPT1b) and long-chain acyl-CoA synthetase 1 (ACSL1), HFD-induced obesity was ameliorated in the transgenic mice with muscle specific SENP2 overexpression [14]. In pancreatic β cells, SENP2 deSUMOylates dynamin-related protein 1 (DRP1) to increase DRP1 phosphorylation, and in turn improves mitochondrial function and insulin secretion upon metabolic stress [15].

Previous studies have demonstrated the effect of SENP2 in the early stages of adipogenesis in BAT and white adipose tissue (WAT) [16, 17]. However, SENP2 is highly expressed in adipose tissue not only in the early stages of development but also in mature adult stage [18]. We recently demonstrated that in WAT, SENP2 is intimately involved not only during the process of adipogenesis but also in maintaining white adipocyte identity through stabilization of C/EBPβ [18]. Specifically, when *Senp2* was knocked out from both BAT and WAT using *Adipoq* (encoding adiponectin)-Cre (*Senp2*-aKO), browning was induced in WAT, exerting a beneficial effect on whole-body metabolism.

Intriguingly, while the metabolic phenotype was improved in the *Senp2*-aKO owing to the browning of WAT, whitening of BAT was observed upon HFD feeding. White-like unilocular adipocytes outnumbered the typical multilocular brown adipocytes when the mice were fed with HFD, suggesting that BAT of HFD-fed *Senp2*-aKO mice are not able to efficiently utilize lipid during energy overload. However, no study has yet investigated the metabolic effect of SENP2 in mature BAT.

In this study, I have generated BAT-specific knockout mice using *Ucp1*-Cre (*Senp2*-BKO) to address the metabolic role of SENP2 in BAT. I examined the phenotypes both at basal condition and in the context of HFD. As heat production is the principal function of BAT, thermogenic response was also inspected during acute cold exposure.

2. Methods and Materials

Mice

All animal experiments in this study were performed in compliance with protocols approved by the Institutional Animal Care and Use Committee (IACUC) at Seoul National University Bundang Hospital (IACUC No. 20-2011-C1A0, IRB number 3520160103). Mice bearing a LoxP-flanked *Senp2* allele (*Senp2*$^{flox/+}$ mice) were generated by the inGenious Targeting Laboratory (Stony Brook, NY, USA). *Ucp1*-Cre transgenic mice were purchased from Jackson Laboratory. Brown adipose tissue *Senp2* conditional knockout mice was generated by serially crossing *Senp2*$^{f/f}$ mice with *Ucp1*-Cre transgenic mice.

Experiments were conducted using 12–24-week-old male mice. Unless otherwise specified, mice were housed at 22–24°C, maintained on a 12-hour light/dark cycle, and had *ad libitum* access to standard pelleted chow or high-fat diet (HFD; 58 kcal% fat with sucrose, D12331; Research Diets, New Brunswick, NJ, USA) and water. Body weight was measured weekly, and food and water intake were calculated by weighing the food/water given and remaining. For mice fed with HFD, HFD was started in 8-week-old mice and were continued for 12 weeks. Body composition was assessed by dual-energy X-ray absorptiometry (DXA), LUNAR Prodigy scanner with software version 8.10 (GE Healthcare, PA, USA). Oxygen consumption, carbon dioxide production, heat production, and locomotor activity were measured using Comprehensive Lab Animal Monitoring System (CLAMS; Columbus Instruments, Columbus, OH, USA).

Acute cold exposure

For cold exposure experiments, mice were placed in 4°C chamber and core body temperature was measured using rectal probe attached to a digital thermometer. Mice had free access to

water only and were sacrificed immediately after 6 hours of cold exposure for analysis.

Glucose and insulin tolerance test

For glucose tolerance test (GTT), mice fasted for 16 hours were intraperitoneally (IP) injected with glucose (2 and 1 g/kg body weight for mice fed with chow diet and HFD, respectively). For insulin tolerance test (ITT), mice fasted for 6 h were IP injected with human insulin (1 U/kg body weight). Blood glucose levels were measured at 0, 15, 30, 60, and 120 minutes from tail vein using OneTouch Ultra glucometer (LifeScan, Milpitas, CA, USA).

Laboratory parameters

Serum insulin level was assessed with Mouse Ultrasensitive Insulin ELISA kit (ALPCO, NH, USA) using 25 μL and 5 μL serum for mice fed with chow diet and HFD, respectively. Triacylglycerol (TG) levels (Cayman Chemical, Ann Arbor, MI, USA) and free fatty acid (FFA) levels (BioVision, CA, USA) were determined by colorimetric assays.

RNA Sequencing

Total RNA of the BAT was isolated using RNeasy mini kit (QIAGEN, Hilden, Germany) according to the manufacturer's protocol. RNA-Seq libraries were prepared by TruSeq Stranded mRNA LT Sample Prep Kit (Illumina). The libraries were sequenced, and the reads were aligned to mouse transcriptome (UCSC gene) and genome (mm10) references, respectively, using HISAT2 version 2.1.0 and Bowtie2 2.3.4.1. Trimming tasks for illumina paired-end and single ended data of each sample's FASTQ files was performed using Trimmomatic 0.38. Transcript assembly was performed using the StringTie program and RLE normalization was processed after filtering the genes with low quality. Specifically, genes with more than 50% of 0 read counts were excluded from the

analysis. From the read counts and Transcripts Per Kilobase Million (TPM), differential gene expression analysis was performed with DESeq2 R statistical package using the criteria of |log2 fold change| ≥ 2 and nbinomWaldTest raw $P < 0.05$. Gene Set Enrichment Analysis (GSEA) were utilized to retrieve Gene Ontology (GO) and Kyoto Encyclopedia of Genes and Genomes (KEGG) pathway data.

Western blot analysis

Tissues and cells were lysed in 20 mM pH 7.4 Tris-HCl, 1 0 mM $Na_4P_2O_7$, 100 mM NaF, 2 mM Na_3VO_4, 1% NP-40 buffer supplemented with protease inhibitor (10 μg/μl aprotinin, 10 μg/μl luepeptin and 1 mM PMSF). The lysates were sonicated two times for 15 seconds each, and the supernatant was collected and quantified after removing cell debris by centrifugation (13,000 rpm for 30 min at 4°C). A total of 5 μg BAT proteins were separated on the SDS-PAGE. Separated proteins were transferred onto nitrocellulose membrane (Whatman, Dassel, Germany). The membrane was blocked with 5% skim milk in Tween20-Tris-buffered saline for 1 hour at room temperature and incubated with the specific primary antibody for overnight at 4°C. Membranes were probed with specific antibodies and bands were visualized by enhanced chemiluminescence (Pierce, IL, USA).

Histological analysis

Tissues were harvested and fixed with 4% paraformaldehyde (Biosesang, Gyeonggi-do, Korea) overnight at 4°C, dehydrated, paraffin-embedded, and sectioned prior to hematoxylin and eosin (H&E) staining. Paraffin-embedded sections of brown and white adipose tissues were subjected to immunohistochemistry staining with PLIN 1 (Santa Cruz, CA, USA) and UCP1 (1:100, Abcam, Cambridge, UK) antibodies according to the manufacturer's instructions. Images were acquired using Upright microscope (NIKON, ECLPSE Ci-L, NY, USA) and diameters of lipid droplets

were measured using Leica software.

Statistical analysis

All animal experiments were repeated at least twice and reproduced. Statistical analyses were performed using IBM SPSS Statistics (version 28.0; IBM Corp., Armonk, NY) and R, version 4.1.2 (The R Foundation for Statistical Computing, Vienna, Austria) (https://www.R-project.org). All data are represented as mean ± s.e.m. unless otherwise specified. Unpaired Student's t-tests were used for two-group comparisons. One-way ANOVA followed by the Tukey's test was used for multiple-group comparisons. The statistical parameters and mouse numbers used per experiment are specified in the figure legends. $P < 0.05$ was considered to be significant throughout the study.

3. Results

Loss of SENP2 in mature BAT does not affect adipogenesis

To elucidate the metabolic role of SENP2 in brown adipocytes *in vivo*, Cre/loxP system was used to generate BAT-specific *Senp2* knockout mouse (*Senp2*-BKO). Specifically, exon 3 of *Senp2* was deleted by breeding the *UCP1*-Cre driver strain with a *Senp2*$^{f/f}$ mouse strain (Figure 1). When compared to the *Senp2*$^{f/f}$ littermates, the expression of *Senp2* was selectively and markedly reduced in BAT of the *Senp2*-BKO, without affecting other members of *Senp* family in BAT (Figure 2A, B).

In the mice fed with standard chow diet, both the control groups and the *Senp2*-BKO mice showed similar patterns of food and water intake (Figure 3A). There was no difference in the body weight nor in the body composition (Figure 3B, C). The respiratory and metabolic parameters were also similar between the groups (Figure 4A, B, C). When examined at 12-weeks of age, BAT as well as other organs including inguinal WAT, epididymal WAT, and liver were morphologically similar, and their mass did not differ between the two groups (Figure 5A, B). Histological analysis showed typical multilocular lipid droplets in the BAT of both groups (Figure 6).

The gene expression profile showed similar levels of *Fabp4* and *Pparg*, implying a similar extent of adipogenesis between the two groups (Figure 7). The levels of *Ucp1* and *Cidea* were slightly decreased in *Senp2*-BKO mice, although *Ucp1* narrowly eluded statistical significance ($P = 0.053$).

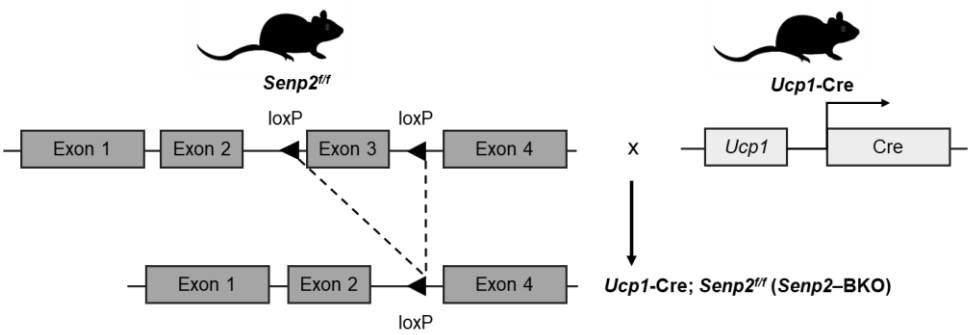

Figure 1. Generation of *Senp2*−BKO mouse

Senp2 brown adipocyte specific−knockout mice (*Senp2*−BKO) were generated by mating *Senp2*$^{flox/flox}$ with *Ucp1*−Cre transgenic mice (Jackson lab). Specifically, a targeting vector was generated using a BAC clone (C57BL/6, RPC23:255D9 clone) containing an 8.36 kb fragment of *Senp2* genomic DNA. Six independent *Senp2*$^{flox/+}$ embryonic stem cell clones were identified and injected into C57BL/6 blastocysts to generate chimeric mice. The chimeric mice were bred with wild type C57BL/6 mice for germline transmission. Heterozygous mice were then crossed with Flipper mice expressing flp−recombinase in the germline (Jackson lab, USA) to delete the FRT−flanked Neo cassette to create the desired *Senp2*$^{flox/+\ allele}$.

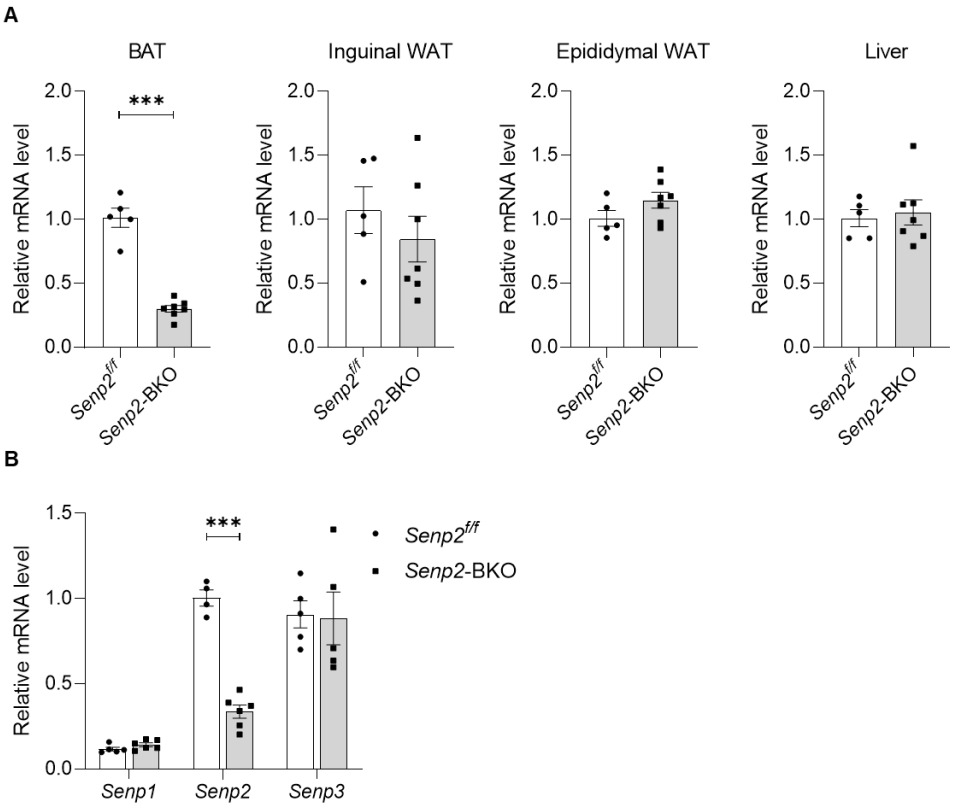

Figure 2. Expression of *Senp2* in *Senp2*$^{f/f}$ and *Senp2*−BKO mice

Fig 2A. Expression of *Senp2* in adipose tissues and liver. *Senp2* was selectively knocked out in brown adipose tissue (BAT).

Fig 2B. Expression of *Senp* family in *Senp2*$^{f/f}$ and *Senp2*−BKO mice.

***, $P < 0.005$

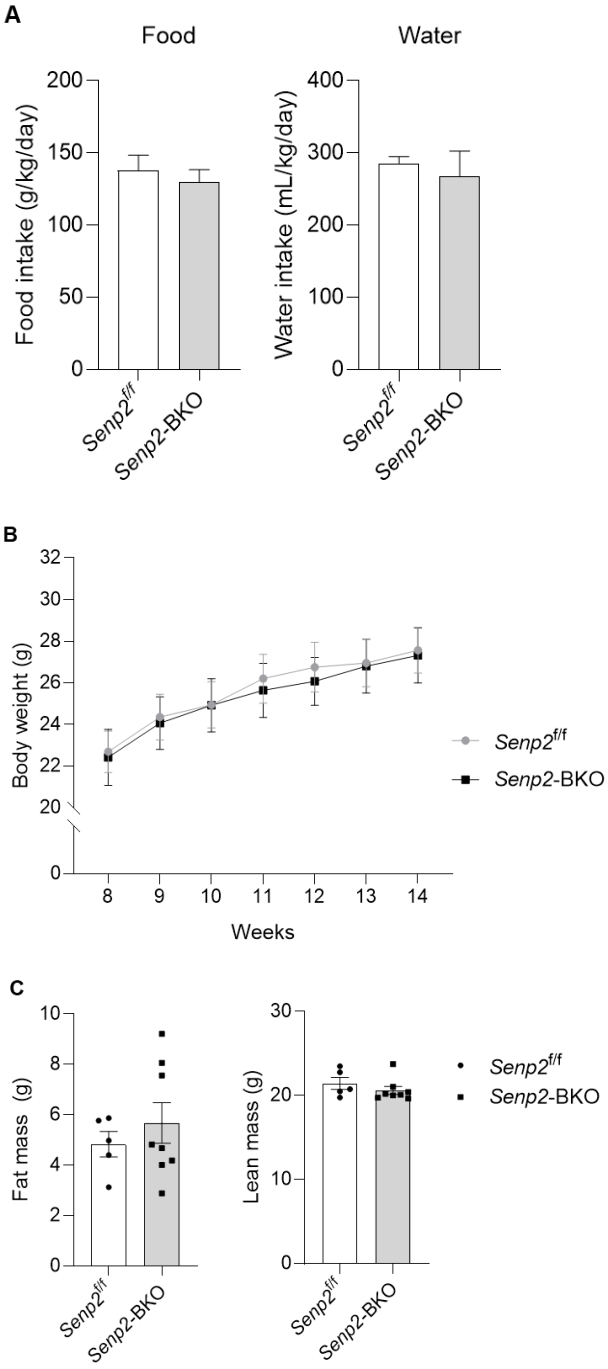

Figure 3. *Senp2*−BKO and *Senp2*$^{f/f}$ mice on standard chow diet

Fig 3A. Average food and water intake in mice fed with standard

chow diet (n = 6–8)

Fig 3B. Body weights of *Senp2*$^{f/f}$ and *Senp2*−BKO mice on standard chow diet (n = 5–8)

Fig 3C. Fat mass and lean tissue of *Senp2*$^{f/f}$ and *Senp2*−BKO mice on standard chow diet (n = 5–8), measured with Bruker's minispec Body Composition Analyzer

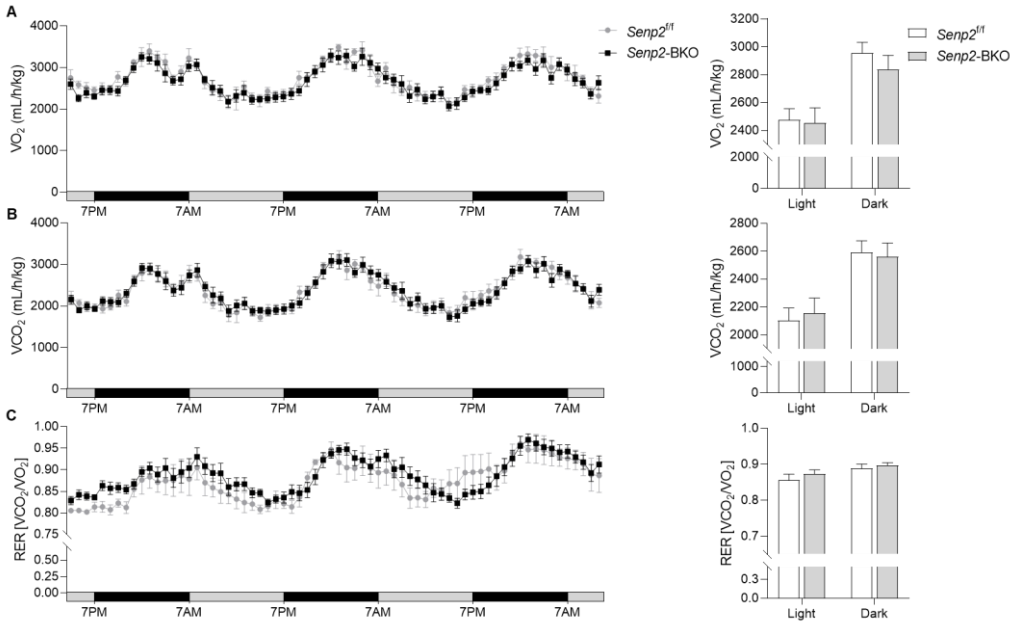

Figure 4. Metabolic cage study

Mice fed with standard chow diet were placed into individual cages in the Comprehensive Laboratory Animal Monitoring System (CLAMS) for 3 days (n = 5–8).

Fig 4A. Volume oxygen (O_2) consumption rates

Fig 4B. Volume carbon dioxide (CO_2) production rates

Fig 4C. Respiratory exchange ratio (RER)

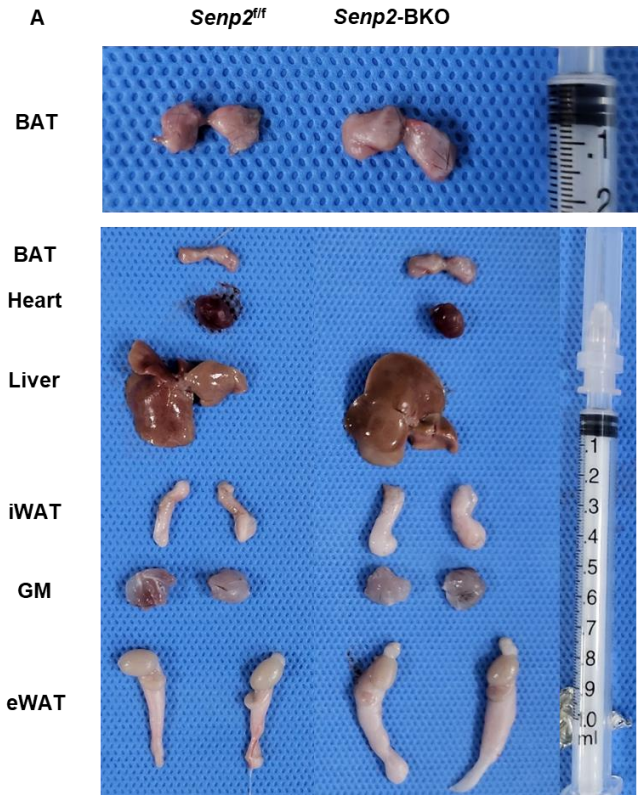

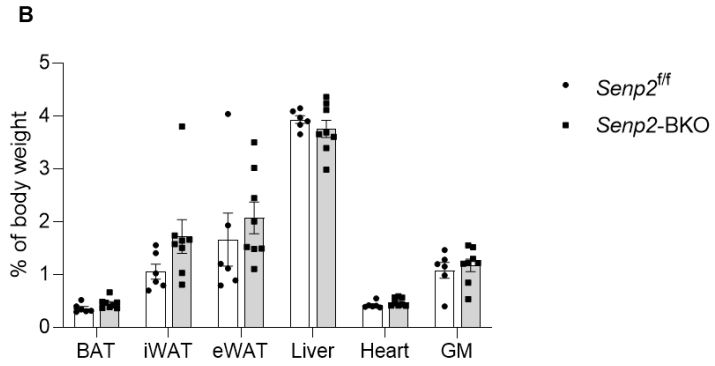

Figure 5. Organ morphology and mass

Fig 5A. Representative photograph of brown adipose tissue (BAT), heart, liver, inguinal white adipose tissue (iWAT), gastrocnemius (GM), and epididymal white adipose tissue (eWAT) of *Senp2*$^{f/f}$ and *Senp2*−BKO mice at 12−weeks. A 1 cc syringe is included for comparison of size.

Fig 5B. Organ weight was expressed as percentage of body weight (n = 5–8).

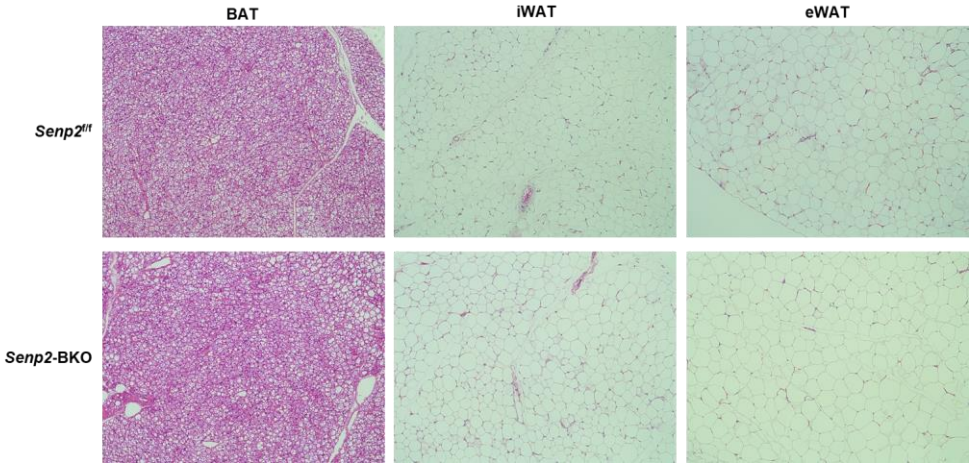

Figure 6. Representative hematoxylin and eosin (H&E) staining of BAT, iWAT and eWAT from *Senp2*$^{f/f}$ and *Senp2*-BKO mice after standard chow diet

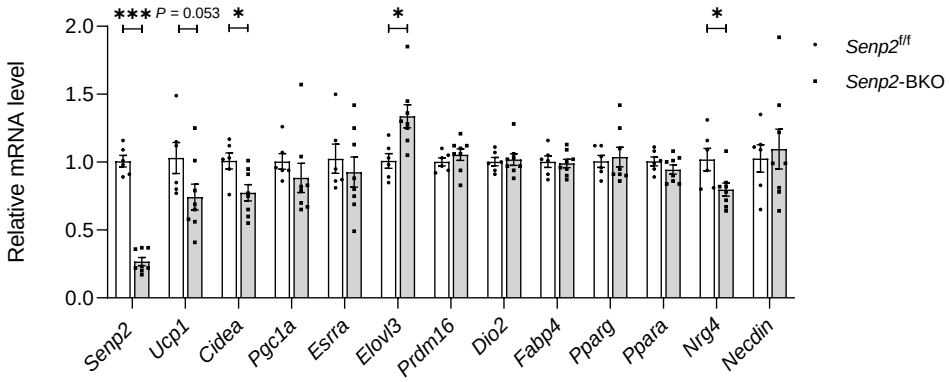

Figure 7. Gene expression profile of BAT in *Senp2*$^{f/f}$ and *Senp2*−BKO mice fed with standard chow diet

qPCR analysis demonstrates decreased expression of *Senp2* and *Cidea*. *Ucp1* narrowly eluded statistical significance. Mann−Whitney U test was used for comparison. $*P < 0.05$, $***P < 0.001$

Senp2-BKO is metabolically distinguishable from Senp2$^{f/f}$ in transcriptome analysis

Many transcription factors are recognized as SUMOylation targets. SENP2 is predominantly located in the nucleus, capable of regulating activities of a number of transcription factors through deSUMOylation [19]. Whereas the direct target protein levels of SENP2 remain unaltered, expression of numerous genes can be regulated by SENP2.

To evaluate the metabolic role of *Senp2* in BAT on a genome-wide level, I analyzed the global transcriptional changes associated with metabolism by performing RNA-sequencing in the BAT of *Senp2*$^{f/f}$ and *Senp2*-BKO mice fed with standard chow diet. Of the 8 samples, 4 from each group, one sample from the *Senp2*-BKO group was an obvious outlier when visualized with the correlation matrix, hierarchical clustering, and multidimensional scaling for all samples (Figure 8A, B, C, D). The transcriptome analysis of BAT was nicely separated after excluding the outlier, and thus subsequent analysis was performed using 4 samples from the *Senp2*$^{f/f}$ and 3 samples from the *Senp2*-BKO group (Figure 9A, B, C, D).

There were 17,817 expressed genes in the processed data and a total of 3,679 genes were differentially expressed: 1,845 upregulated and 1,834 downregulate genes. A KEGG enrichment analysis revealed that these differentially expressed genes were most significantly related to pathways regarding metabolism, thermogenesis, p38 mitogen-activated protein kinase (MAPK) signaling pathway, fatty acid metabolism, PPAR signaling pathway, and oxidative phosphorylation (Figure 10A, B).

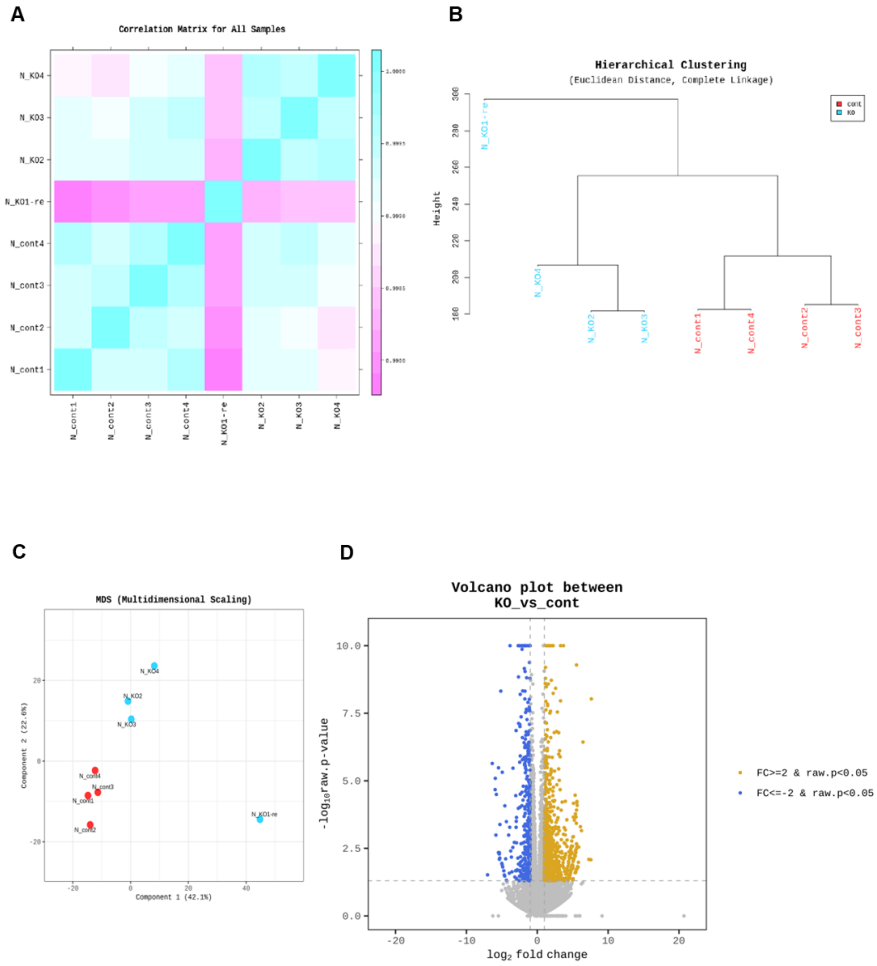

Figure 8. Correlogram of all RNA-seq samples

Fig 8A. Correlation matrix for all samples

Fig 8B. Hierarchial clustering. Euclidean distance was used for distance metrics and complete linkage was used as a linkage method.

Fig 8C. Principal component analysis of RNA-seq data revealed an outlier.

Fig 8D. Volcano plot between *Senp2*$^{f/f}$ and *Senp2*-BKO mice groups N_cont1, N_cont2, N_cont3, N_cont4 are from the *Senp2*$^{f/f}$ mice and N_KO1_re, N_KO2, N_KO3, and N_KO4 are from the *Senp2*-BKO mice group. N_KO1_re sample was prepared at a different timepoint due to the substandard RNA quality.

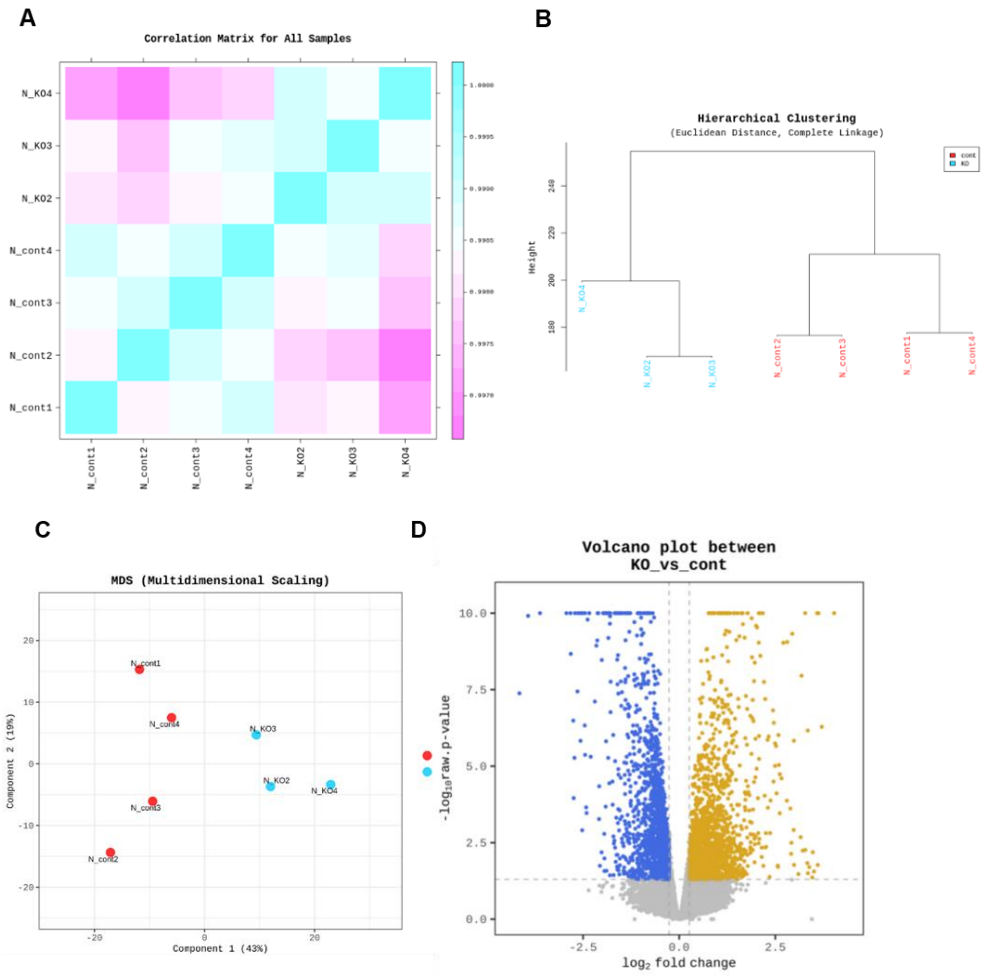

Figure 9. Correlogram of selected RNA-seq samples

Fig 9A. Correlation matrix for selected samples (N = 4 for the *Senp2*$^{f/f}$ group and N = 3 for the *Senp2*-BKO mice group)

Fig 9B. Hierarchial clustering. Euclidean distance was used for distance metrics and complete linkage was used as a linkage method.

Fig 9C. Principal component analysis of RNA-seq data

Fig 9D. Volcano plot between *Senp2*$^{f/f}$ and *Senp2*-BKO mice groups N_cont1, N_cont2, N_cont3, N_cont4 are from the *Senp2*$^{f/f}$ mice and N_KO1_re, N_KO2, N_KO3, and N_KO4 are from the *Senp2*-BKO mice group. N_KO1_re sample excluded considering the batch effect.

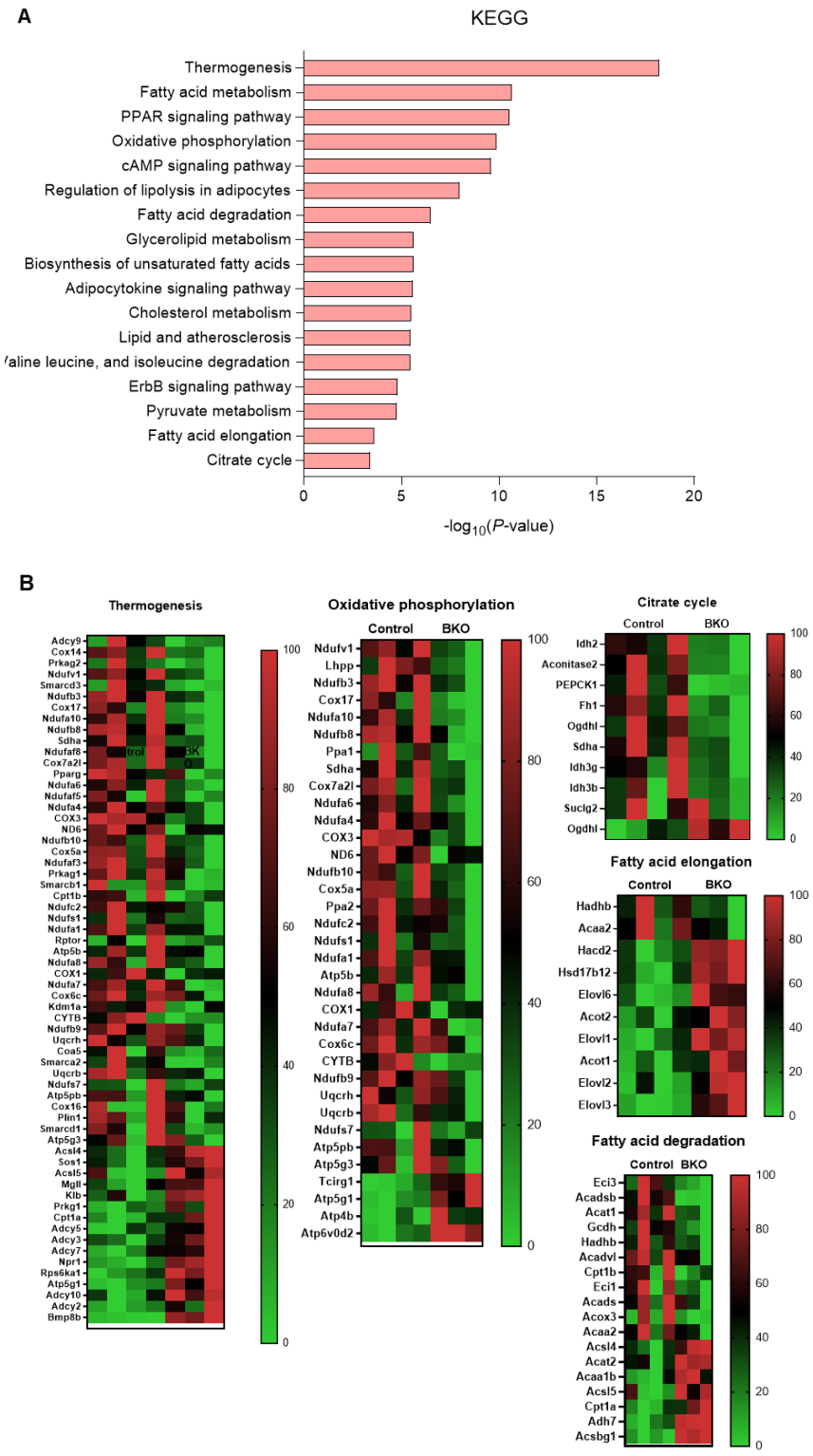
A
KEGG
Thermogenesis
Fatty acid metabolism
PPAR signaling pathway
Oxidative phosphorylation
cAMP signaling pathway
Regulation of lipolysis in adipocytes
Fatty acid degradation
Glycerolipid metabolism
Biosynthesis of unsaturated fatty acids
Adipocytokine signaling pathway
Cholesterol metabolism
Lipid and atherosclerosis
Valine leucine, and isoleucine degradation
ErbB signaling pathway
Pyruvate metabolism
Fatty acid elongation
Citrate cycle
0
5
10
15
20
-log10(P-value)
B
Thermogenesis
Control
BKO
Oxidative phosphorylation
Control
BKO
Citrate cycle
Control
BKO
Fatty acid elongation
Control
BKO
Fatty acid degradation
Control
BKO

Figure 10. Differentially expressed genes in the BAT of *Senp2*$^{f/f}$ and *Senp2*−BKO mice

Fig 10A. Comparing top Gene Ontology (GO) Kyoto Encyclopedia of Genes and Genomes (KEGG) terms associated with *Senp2*−responsive genes in BAT. Enrichment analysis was performed using differentially expressed genes in BAT between *Senp2*$^{f/f}$ and *Senp2*−BKO mice groups.

Fig 10B. Heatmap of top GO KEGG annotation terms in BAT between *Senp2*$^{f/f}$ and *Senp2*−BKO mice groups.

Senp2-BKO mice exhibit insulin resistance upon HFD feeding

Mice fed with standard chow diet showed comparable blood glucose levels between the groups, both at fed and fasting state (Figure 11A, B). *Senp2*-BKO mice exhibited similar glucose intolerance and insulin resistance when compared with *Senp2*$^{f/f}$ littermates (Figure 12A, B).

When mice were fed with HFD, however, the random glucose started to diverge at 12 weeks (Figure 13). *Senp2*-BKO mice exhibited increased systemic glucose intolerance when IP-GTT was performed at 13 weeks of HFD (Figure 14A). *Senp2*-BKO mice were more insulin resistant on the IP-ITT performed at 14 weeks than controls (Figure 14B), despite no difference in body weight or fat portion (Figure 15A, B).

As seen in the BAT of *Senp2*-aKO mice, a mixed population of unilocular and multilocular adipocytes were observed in the BAT of *Senp2*-BKO mice fed with HFD, suggesting diminished BAT function in response to SENP2 deficiency (Figure 16). BAT activity is associated with a healthy metabolic profile including enhanced insulin sensitivity. Therefore, the above findings are indicative of loss of multilocular organization as well as deteriorated BAT function in *Senp2*-BKO mice in response to dietary overload.

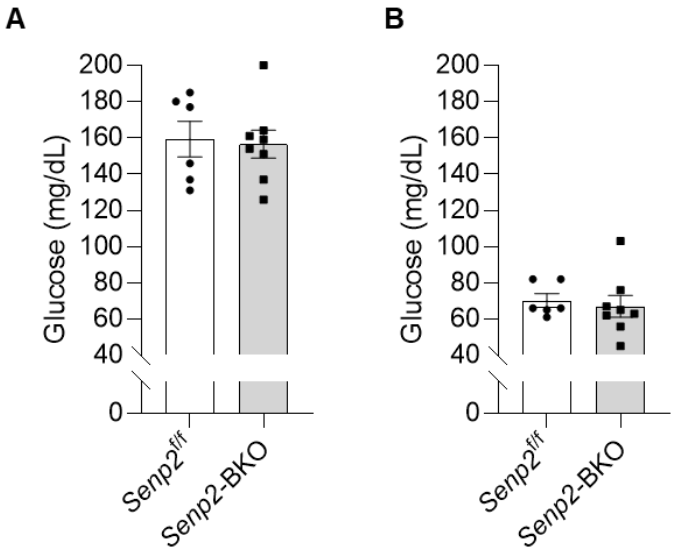

Figure 11. Serum glucose levels of *Senp2*$^{f/f}$ and *Senp2*−BKO mice fed with standard chow diet

Fig 11A. Random glucose of *Senp2*$^{f/f}$ and *Senp2*−BKO mice in fed state (N = 6–8)

Fig 11B. Fasted glucose of *Senp2*$^{f/f}$ and *Senp2*−BKO mice (N = 6–8)

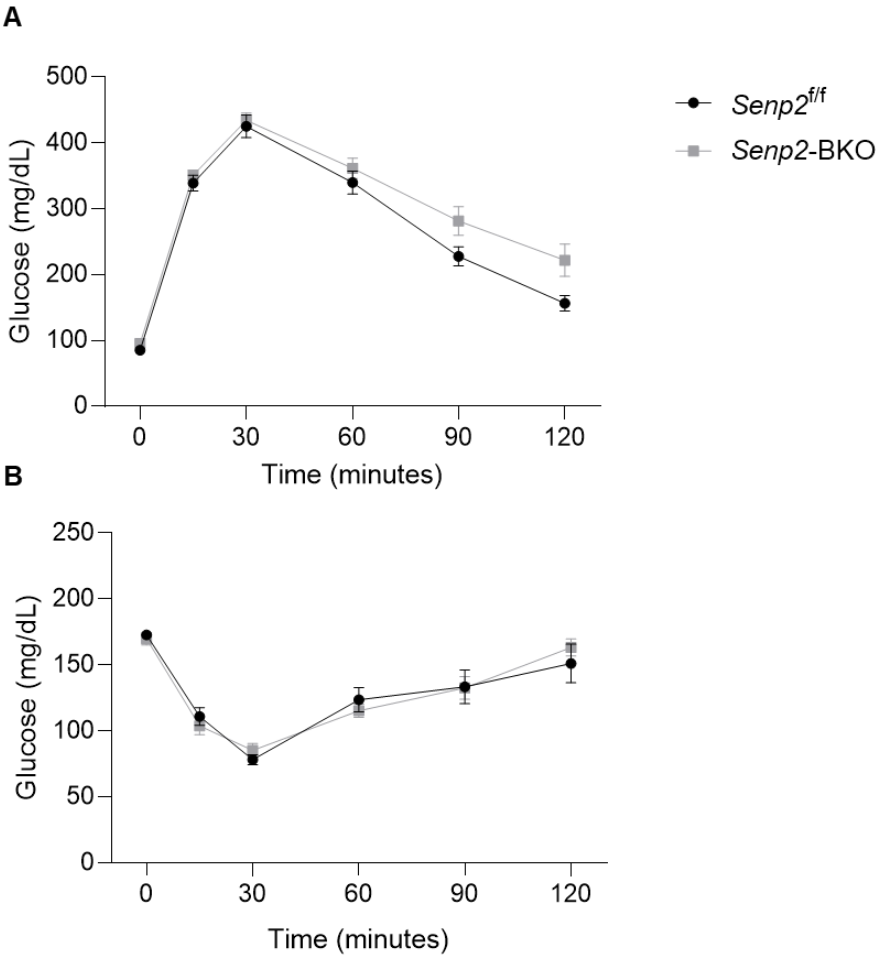

Figure 12. Comparable glucose profiles of *Senp2*$^{f/f}$ and *Senp2*−BKO mice fed with standard chow diet

Fig 12A. Glucose tolerance test of *Senp2*$^{f/f}$ and *Senp2*−BKO mice (N = 5–8)

Fig 12B. Insulin tolerance test of *Senp2*$^{f/f}$ and *Senp2*−BKO mice (N = 5–8)

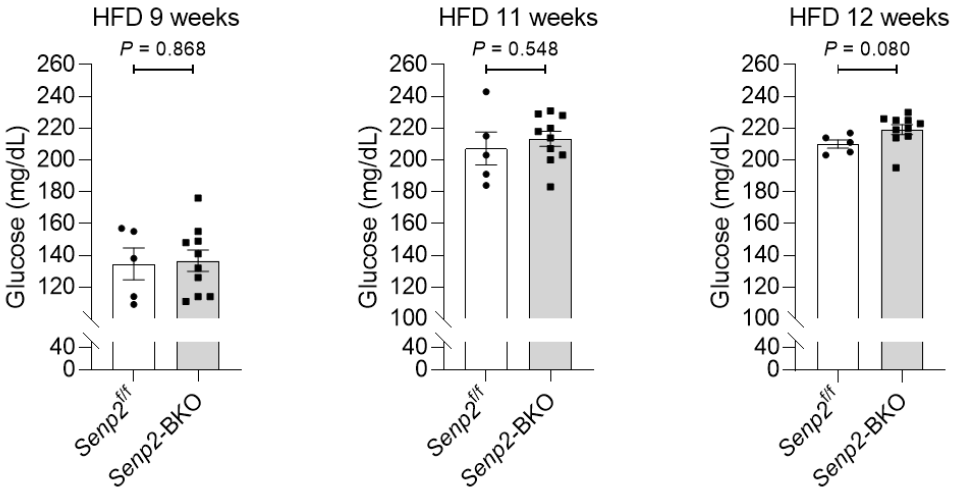

Figure 13. Random glucose of *Senp2*$^{f/f}$ and *Senp2*−BKO mice fed with high fat diet (HFD) (N = 5–10)

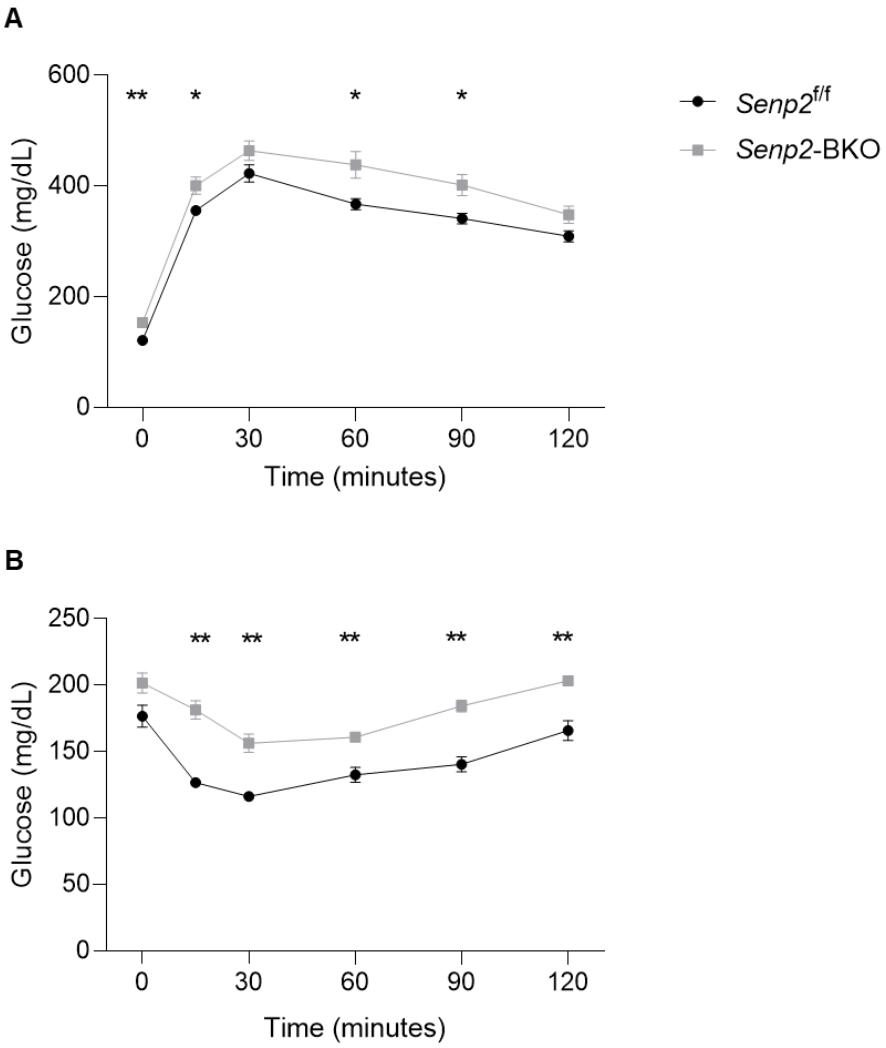

Figure 14. *Senp2*−BKO mice are more insulin resistant than *Senp2*$^{f/f}$ mice when fed with HFD

Fig 14A. Glucose tolerance test of *Senp2*$^{f/f}$ and *Senp2*−BKO mice at 13 weeks of HFD feeding (N = 5–10)

Fig 14B. Insulin tolerance test of *Senp2*$^{f/f}$ and *Senp2*−BKO mice at 14 weeks of HFD feeding (N = 5–10)

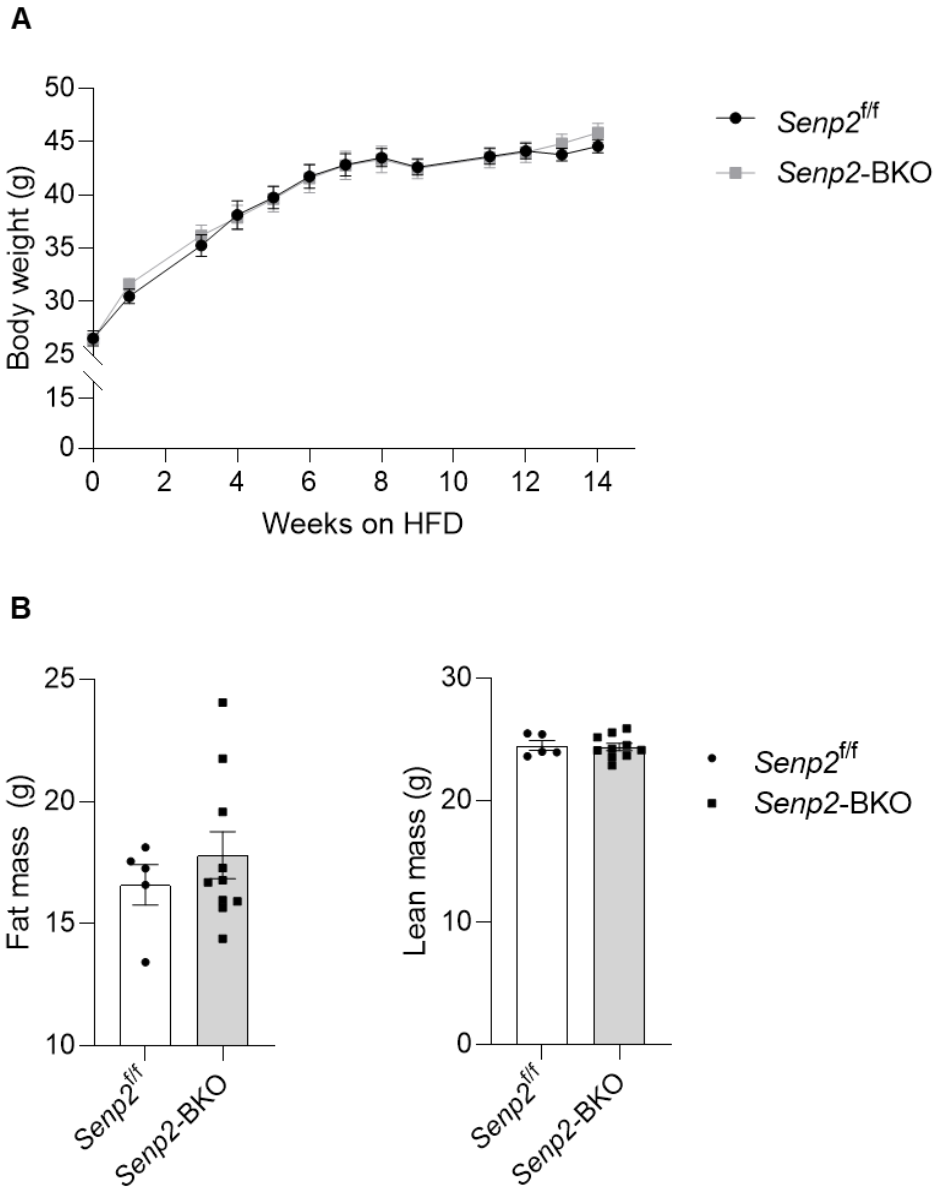

Figure 15. Body weights and composition of *Senp2*$^{f/f}$ and *Senp2*−BKO mice fed with HFD

Mice were fed with HFD from the age of 8 weeks

Fig 15A. Body weights of *Senp2*$^{f/f}$ and *Senp2*−BKO mice on HFD (n = 5–10)

Fig 15B. Fat mass and lean mass of *Senp2*$^{f/f}$ and *Senp2*−BKO mice fed with HFD for 14 weeks (n = 5–10)

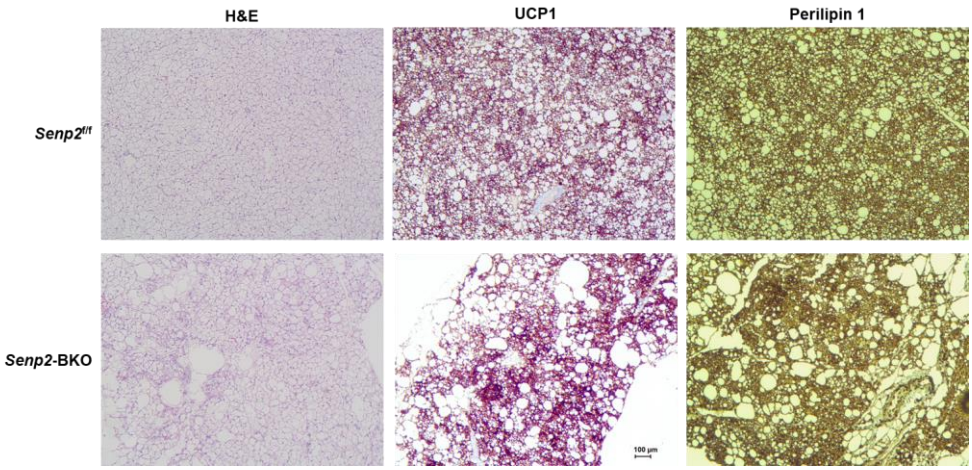

Figure 16. Representative H&E, UCP1 immunohistochemistry (IHC), and Perilipin 1 IHC staining of BAT from *Senp2*$^{f/f}$ and *Senp2*−BKO mice after HFD feeding for 14 weeks

Senp2-BKO mice are intolerant to acute cold exposure

Adaptive thermogenesis is the most prominent feature of BAT. I next asked whether the subtle decrease of thermogenic marker expression at baseline and structural alterations in the BAT of *Senp2*-BKO mice during HFD feeding were also linked to compromise in BAT function during thermogenic demand. To this end, I assessed the thermogenic capacity of *Senp2*$^{f/f}$ and *Senp2*-BKO mice in response to acute cold exposure.

There was no difference in the rectal temperature of *Senp2*$^{f/f}$ and *Senp2*-BKO mice at ambient temperature both at fed and fasted status (Figure 17A), When mice were exposed to 4°C, however, both groups of mice initially maintained body temperature by shivering, but this response was abolished after 2-3 hours (Figure 17B). *Senp2*$^{f/f}$ mice were capable of maintaining core body temperature through non-shivering thermogenesis whereas *Senp2*-BKO mice were severely cold intolerant from three hours of acute cold exposure.

Cold-activated BAT displayed marked increase in expression of genes related to thermogenesis in control mice (Figure 18). Intriguingly, in *Senp2*-BKO mice, the extent of thermogenic gene induction was repressed compared to littermate controls. Similar patterns of activation in thermogenic program upon acute cold exposure were observed in the BAT of *Senp2*-aKO, despite the variation in the extent of *Ucp1* and *Ppargc1a* induction levels (Figure 19).

Taken together, BAT deficient of *Senp2* display defective adaptive thermogenesis as a consequence of inadequate upregulation of thermogenic genes in BAT.

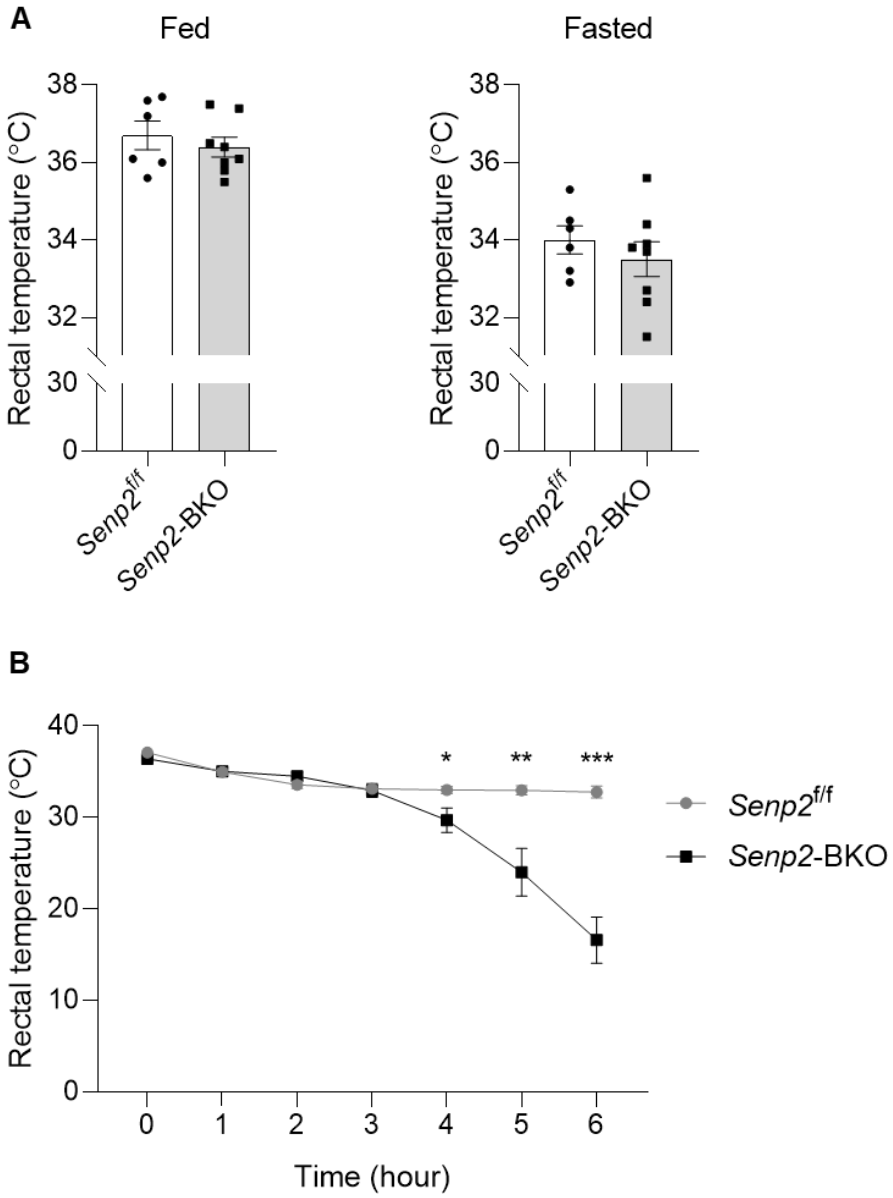

Figure 17. Core body temperature of 12−15 weeks old *Senp2*$^{f/f}$ and *Senp2*−BKO mice fed with standard chow diet

Fig 17A. Core body temperature of *Senp2*$^{f/f}$ and *Senp2*−BKO mice at fed and fasted status at ambient temperature (n = 5-8)

Fig 17B. Core body temperature of *Senp2*$^{f/f}$ and *Senp2*−BKO mice during acute cold exposure at 4°C for 6 hours (n = 5-8)

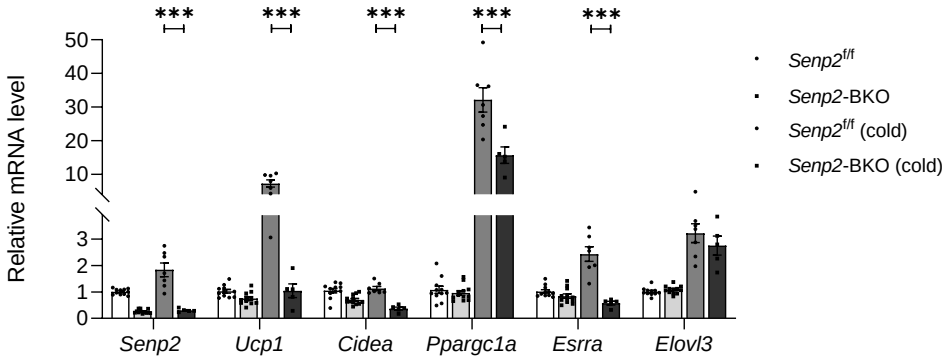

Figure 18. Levels of thermogenic genes were augmented on acute cold exposure and the difference was diverged between the *Senp2*$^{f/f}$ and *Senp2*−BKO mice groups (N = 5-12)

Data are presented as mean ± s.e.m; one−way ANOVA followed by *post hoc* Tukey' s test was used for comparison.

Only the *P* value for the *Senp2*$^{f/f}$ (cold) and *Senp2*−BKO (cold) mice groups are annotated in the figure for simplicity. *** $P < 0.001$

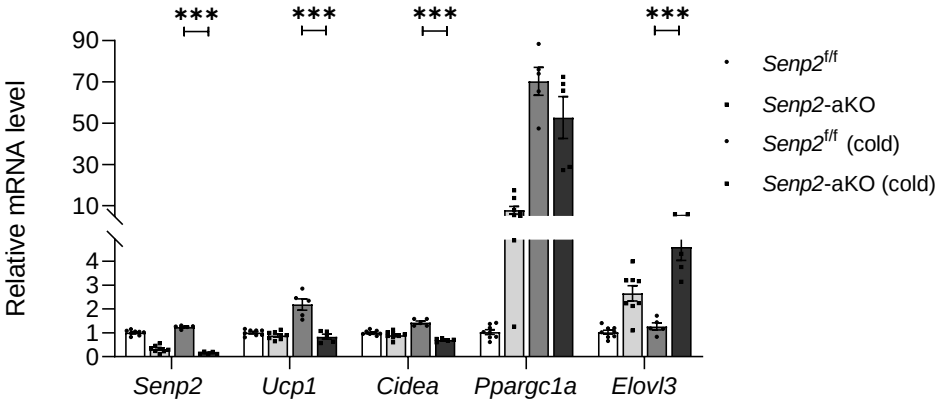

Figure 19. Levels of thermogenic genes were augmented on acute cold exposure and the difference was diverged between the *Senp2*$^{f/f}$ and *Senp2*−aKO (*Adipoq*−Cre) mice groups (N = 5-8)

Data are presented as mean ± s.e.m; one−way ANOVA followed by *post hoc* Tukey' s test was used for comparison.

Only the *P* value for the *Senp2*$^{f/f}$ (cold) and *Senp2*−aKO (cold) mice groups are annotated in the figure for simplicity. *** $P < 0.001$

4. Discussion

Thermogenesis in BAT is principally controlled by norepinephrine, which is released from sympathetic nerve terminals in response to cold exposure or dietary stimuli [20]. This β-adrenergic receptor signaling leads to increase in cyclic adenosine monophosphate (cAMP) and protein kinase A (PKA)-mediated activation of intracellular events including activation of *Ucp1*, triglyceride hydrolysis, and fatty acid oxidation. Although the main substrate that activates BAT thermogenesis is considered to be fatty acid, systemic glucose utilization is concomitantly increased in parallel with UCP1 activation through AMP kinase activation [21]. In this study, I have revealed that despite comparable phenotypes of *Senp2*$^{f/f}$ and *Senp2*-BKO mice fed with standard chow diet, metabolic profiles such as cold tolerance and insulin sensitivity were much inferior in the *Senp2*-BKO mice when exposed to acute cold exposure or HFD-feeding.

I investigated the BAT specific role of SENP2 using the Cre-LoxP system. There was no difference between the groups regarding intrascapular BAT mass, expression of genes related to adipogenesis, and histological analysis, suggesting that *Senp2* knockout using *Ucp1*-Cre did not affect adipogenesis in BAT. In a previous report by Liang et al., conditional BAT-specific SENP2 knockout mice had suppressed brown adipocyte differentiation via disinhibition of Necdin [17]. In the study, myogenic factor 5 (*Myf5*)-Cre was employed to knockout *Senp2* in contrary to our study in which *Ucp1*-Cre was used. When we used *Adipoq*-Cre to knock out *Senp2* in both brown and white adipose tissues, not only was the size of BAT considerably smaller than their littermate *Senp2*$^{f/f}$ mice, but dysfunctional histology was also observed, with lower density of multilocular clusters of intracellular lipid droplets [18]. It is recognized that brown adipocytes are derived from a *Myf5*-expressing progenitors [22], indicating that by using *Myf5*-

Cre, *Senp2* was knocked out in the very early stage of development. The generation of brown adipocytes in BAT starts as early as E10 and finishes by E16 when detected with the AdipoChaser mouse model based on adiponectin promoter [23], but expression UCP1 is BAT specifically induced at E19 in mice [24]. Therefore, it can be safely concluded that by using *Ucp1*-Cre, targeted *Senp2* gene deletion on mature BAT was attainable.

However, while deletion of *Senp2* in mature BAT did not adversely impact adipogenic differentiation or energy expenditure, mice deficient of *Senp2* demonstrated defect in metabolism, especially when exposed to cold stimuli or HFD. It has been reported that UCP1 is essential in confined conditions, i.e., for adaptive adrenergic non-shivering thermogenesis [25]. UCP1-ablated mice had similar body weight and the metabolic rates at both 30°C and at 18°C compared to controls, although UCP1-ablated mice were devoid of adrenergically induced non-shivering thermogenetic actions. In another report that studied noncanonical thermogenic mechanism, *Prdm16* transgenic (Tg) mice and *Prdm16* Tg × *Ucp1*$^{-/-}$ mice displayed similar core body temperature at baseline compared to their respective littermates without *Prdm16* overexpression but were more capable of maintaining their body temperature under cold conditions [26]. These mice had improved insulin sensitivity in the GTT and ITT at 11 weeks of HFD, but this enhanced glucose disposal was not observed under a standard chow diet. Collectively, thermogenins such as UCP1 is dispensable at subthermoneutral (22–26°C) or thermoneutral (30°C) conditions on balanced intake of energy sources. In the same line, it can be argued that the genuine virtue of BAT and BAT-associated markers from SENP2 arises upon metabolic stress. As considerable amount of metabolically active BAT is also present in adult humans and that metabolic stress is induced by western dietary pattern characterized by high daily intake of carbohydrates and saturated fats, the metabolic role of SENP in BAT in the defense against obesity should be revitalized.

This study has several limitations. The RNA seq results

performed with mice housed at ambient temperature revealed dissimilarity in gene clusters involved in metabolism and thermogenesis. Considering that the subtle reduction of *Ucp1* and *Cidea* gene and slight increase in *Elovl3* in the qPCR analysis was remarkably amplified on acute cold exposure, however, it would be informative and desirable to perform RNA seq with the activated BAT. As some of the cold-induced genes, i.e., *Ppargc1a* and *Esrra*, were not different between the groups at baseline but were repressed in the BAT of *Senp2*-BKO compared to controls upon cold stimuli, analyzing the transcriptome profile after cold exposure would reveal interesting pathways that emphasize the upregulation of thermogenic genes. Also, although UCP1 is the key thermogenin involved in the canonical thermogenic mechanism and regulation of the glucose homeostasis in BAT, UCP1-independent thermogenic mechanisms have been identified [27, 28]. These include creatine-substrate cycling and ATP-dependent Ca^{2+} cycling thermogenesis in beige adipocytes [26, 29]. BAT could also secrete brown adipokines, or batokines, which positively regulate systemic metabolism [30-34]. Nonetheless, I have primarily concentrated on the UCP1-dependent signaling pathway in interpreting the changes in adaptive thermogenesis and glucose homeostasis in *Senp2*$^{f/f}$ and *Senp2*-BKO mice in this study. In the next section, I focused on elucidating the possible mechanisms of which SENP2 could be involved in regulating the expression of UCP1.

Chapter 2.
Mechanism of SENP2 in BAT Metabolism

1. Introduction

In the previous section, I have corroborated the role of SENP2 in BAT metabolism. While SENP2 deficiency resulted in modest reduction of *Ucp1* and *Cidea* in standard chow diet-fed mice at ambient temperature, the effect SENP2 was largely augmented upon metabolic stress: HFD and acute cold exposure.

It is well established that in response to cold stimuli, adaptive thermogenesis of brown adipose tissue is regulated by activation of β3 adrenergic receptor through the cAMP signaling cascade [35]. In the course of cAMP signaling mechanism, MAPK serves as a central mediator in the transcription of *Ucp1* gene by phosphorylating transcription regulators that directly act at the *Ucp1* promoter, i.e., activating transcription factor 2 (ATF-2) and cAMP-responsive element binding protein (CREB). Activation of ATF-2 by p38 MAPK as well as p38 MAPK *per se* additionally increases the expression of PPARγ coactivator 1α (PGC-1α, encoded by *Ppargc1a*), a key regulator of energy metabolism [36]. The prominence of PGC-1α cannot be emphasized enough, functioning as a master transcriptional coregulator of energy metabolism including not only adaptive thermogenesis but also mitochondrial biogenesis, oxidative phosphorylation, and fatty acid elongation/degradation [37-39]. These pleiotropic actions of PGC-1α are orchestrated through interaction with several nuclear receptor targets: namely, PPARγ, PPARα, nuclear respiratory factor (NRF)-1, NRF-2, liver X receptor (LXR) and estrogen-related receptor α (ERRα) [39-45].

ERRα is an orphan receptor of which the role is underappreciated [46, 47]. It is known to exert synergistic effect with the coactivation of PGC-1α to activate *Ucp1* and Sirtuin 3

(*Sirt3*) gene transcription as well as inducing mitochondrial biogenesis [48-51]. Both ERRα and PGC-1α are SUMOylated proteins, and their levels are increased upon cold exposure [52]. Mouse deficient on all forms of ERRs show defect in adaptive thermogenesis, however no study has yet revealed how regulation of ERRα activity by post-translational modification may affect BAT.

Here, I aimed to identify the potential *in vitro* mechanisms of how SENP2 deficiency may downregulate the levels of *Ucp1* and *Cidea* in brown adipocytes, particularly focusing on the coactivation of ERRα and PGC-1α.

2. Methods and Materials

Cell culture

Mouse brown preadipocytes (a kind gift from Dr. Shingo Kajimura, Beth Israel Deaconess Medical Center and Harvard Medical School, Boston, MA, USA) were maintained in high glucose Dulbecco's Modified Eagle's Medium (DMEM) (Sigma Aldrich, St. Louis, MO, USA) supplemented with 10% fetal bovine serum (FBS) and 100 U/mL Penicillin-Streptomycin (ThermoFisher, Waltham, MA, USA) at 37°C in a humidified atmosphere with 5% CO_2. Differentiation of brown adipocytes was induced by treating 95% confluent preadipocytes with DMEM containing 10% FBS and 1% penicillin-streptomycin, 0.5 μM rosiglitazone, 1 nM T3, 850 nM insulin, 125 nM indomethacin, 2 μg/ml dexamethasone, and 0.5 mM isobutylmethylxanthine. Two days after induction, cells were switched to maintenance medium containing 10% FBS and 1% penicillin-streptomycin, 1 nM T3, and 850 nM insulin. Mouse brown adipocytes were fully differentiated 6 days after inducing differentiation.

Reverse siRNA transfection

To enhance transfection efficiency without interfering with adipogenesis, target genes were knocked down on day 4 of brown preadipocyte differentiation using reverse siRNA transfection method and were harvested on day 6. Lipofectamine RNAiMAX (Invitrogen, Waltham, MA, USA) and siRNA were diluted separately in serum free DMEM, and 250 μL of each reagent was added to gelatin-coated 12-well cell culture plates to be incubated for 25 minutes at room temperature. The final concentrations of lipofectamine RNAiMAX and siRNA were 2.5 μL/mL and 50 nM, respectively.

During incubation, cells were detached with 0.05% Trypsin-

EDTA (#25300054, GIBCO, Grand Island, NY, USA) for 2 minutes, centrifuged (3,000 rpm, 5 min), and resuspended in the culture medium containing 2 nM T3 and 1,700 nM insulin. On top of the pre-incubated siRNA-RNAiMAX complex, 500 μL of the cell suspension were added. The final concentrations of T3 and insulin were the same as the maintenance media. The replated cells were further cultured for 2 days without changing media and were harvested for analysis.

Oil Red O staining

Fully differentiated brown adipocytes were washed once with PBS and fixed with 10% paraformaldehyde for 15 minutes. The cells were washed with distilled water for two times and 100% propylene glycol (Sigma-Aldrich) was added and suctioned out after 5 minutes. Subsequently, cells were stained with Oil-Red-O solution (0.5% in propylene glycol, O1516, Sigma-Aldrich) for 30 minutes at ambient temperature. The cells were washed with 85% propylene glycol solution for 3 minutes, washed twice with distilled water, and the stained samples were visualized with light microscope.

Immunofluorescent staining

Fully differentiated adipocytes were stained with 100 nM MitoTracker Red FM (Invitrogen, Carlsbad, CA, USA) for 30 min to label mitochondria. Cell nuclei were then counterstained with 300 nM of DAPI stain solution. The fluorescent signal was observed using a confocal microscope (LSM 510META, Carl Zeiss, Oberkochen, Germany).

RNA preparation and real-time PCR

Total RNA was isolated from cells using TRIzol (Invitrogen) according to the manufacturer's instructions. RNA samples were reverse-transcribed using the High Capacity cDNA Reverse

Transcription Kits (Applied Biosystems, Waltham, MA, USA): 10 μL of 100 ng/μL RNA was mixed with 2 μL of 10X RT buffer, 2 μL of 10X RT random primers, 0.8 μL of 25X dNTP mix (100 mM), 1 μL of MultiScribe Reverse Transcriptase (50 U/μL), and 1 μL of RNase inhibitor (20 U/μL). Reverse transcription was performed by incubating the mixture at 25℃ for 10 minutes, 37℃ for 120 minutes, followed by 85℃ for 5 minutes. Real-time PCR was carried out in 96-well plates using TaqMan Master Mix reagents and a TaqMan ABI PRISM 7000 sequence detector system (Applied Biosystems). 36B4 RNA was used as an endogenous control. Analysis was performed in duplicates and repeated at least three times.

Table 1. List of the primers used for qPCR

	Forward	Reverse
Senp2	5' CAG TCT CTA CAA TGC TGC CAG 3'	5' CCA GAA GGG GCC ACA TTC 3'
Ucp1	5' ACT GCC ACA CCT CCA GTC ATT 3'	5' CTT TGC CTC ACT CAG GAT TGG 3'
Cidea	5' TGA CAT TCA TGG GAT TGC AGA C 3'	5' GGC CAG TTG TGA TGA CTA AGA C 3'
Elovl3	5' TTC TCA CGC GGG TTA AAA ATG G 3'	5' GAG CAA CAG ATA GAC CAC 3'
Dio2	5' CAG TGT GGT GCA CGT CTC CAA TC 3'	5' TGA ACC AAA GTT GAC CAC CAG 3'
Pparg	5' GGA AGA CCA CTC GCA TTC CTT 3'	5' GTA ATC AGC AAC CAT TGG GTC A 3'
Ppara	5' TGT CGA ATA TGT GGG GAC AA 3'	5' AAT CTT GCA GCT CCG ATC AC 3'
Ppargc1a	5' ACC TGA CAC AAC GCG GAC AG 3'	5' TCT CAA GAG CAG CGA AAG CG 3'
Prdm16	5' CAG CAC GGT GAA GCC ATT C 3'	5' GCG TGC ATC CGC TTG TG 3'
Necdin	5' CAC TTC CTC TGC TGG TCT CC 3'	5' ATC GCT GTC CTG CAT CTC AC 3'

Esrra	5’ GCA GGG CAG TGG GAA GCT A 3’	5’ CCT CTT GAA GAA GGC TTT GCA 3’
Fabp4	5’ GGG GCC AGG CTT CTA TTC C 3’	5’ GGA GCT GGG TTA GGT ATG GG 3’
Adiponectin	5’ CGA TTG TCA GTG GAT CTG ACG 3’	5’ CAA CAG TAG CAT CCT GAG CCC T 3’
Citrate synthase	5’ CCC CTG CCT GAG GGC TTA T 3’	5’ GCC AAG ACA CCT GTT CCT CTG T 3’
Cox7a1	5’ CAG CGT CAT GGT CAG TCT GT 3’	5’ AGA AAA CCG TGT GGC AGA GA 3’
Cox8b	5’ CTC CCC CCT ATC CTG CGG CTG 3’	5’ ACT ATG GCT GAG ATC CCC ACA 3’
Nrf1	5’ GGC AAC AGT AGC CAC ATT GGC T 3’	5’ GTC TGG ATG GTC ATT TCA CCG C 3’
Mfn1	5’ CCA GGT ACA GAT GTC ACC ACA G 3’	5’ TTG GAG AGC CGC TCA TTC ACC T 3’
Mfn2	5’ GTG GAA TAC GCC AGT GAG AAG C 3’	5’ CAA CTT GCT GGC ACA GAT GAG C 3’
Opa1	5’ TCT CAG CCT TGC TGT GTC AGA C 3’	5’ TTC CGT CTC TAG GTT AAA GCG CG 3’
Drp1	5’ GCG AAC CTT AGA ATC TGT GGA CC 3’	5’ CAG GCA CAA ATA AAG CAG GAC GG 3’
Fis1	5’ GCT GGT TCT GTG TCC AAG AGC A 3’	5’ GAC ATA GTC CCG CTG TTC CTC T 3’
β actin	5’ GAA GCT GTG CTA TGT TGC TCT 3’	5’ GGA GGA AGA GGA TGC GGC A 3’
36B4	5’ GCT TCA TTG TGG GAG CAG ACA 3’	5’ TGC GCA TCA TGG TGT TCT TG 3’
Cytochrome b	5’ CAT TTA TTA TCG CGG CCC TA 3’	5’ TGT TGG GTT GTT TGA TCC TG 3’
18S	5’ CTC AAA GAT TAA GCC ATG C 3’	5’ TTT ACG GTC AGA ACT AGG G 3’

Quantification of the mitochondrial (mt)DNA copy number

Genomic DNA was extracted from differentiated brown adipocytes. Specifically, cells were harvested with 300 μL of cell lysis buffer (QIAGEN, Hilden, Germany) and 1.5 μL of proteinase K (Cat. No. 19131, QIAGEN, Hilden, Germany) and were lysed at 50°C for 2 hours. After vortexing, 100 μL of protein precipitation solution (Qiagen) was added, centrifuged at 13,000 rpm, 4°C for 5 minutes, and supernatants were mixed with the 400 μL of isopropyl alcohol for genomic DNA isolation. Genomic DNA was diluted to final concentrations of 10 ng/mL with DEPC treated water. The mtDNA copy number was amplified using primer for the mitochondrial ND1 gene and normalized to genomic DNA by amplification of the cytochrome b gene.

Measurement of oxygen consumption

Oxygen consumption rate (OCR) was measured using a Seahorse XF24 extracellular flux analyzer (Agilent). The cultured brown adipocytes were detached with 0.05% Trypsin-EDTA (#25300054, GIBCO, Grand Island, NY, USA) on day 4 of differentiation, reverse-transfected with nonsense siRNA (siNS) or siSENP2 as described previously and seeded in a XF24 V7 cell culture microplates (Seahorse Bioscience) to be incubated for two days.

For the measurement of OCR, the basal respiration was assessed in untreated cells for 20 minutes. ATP turnover was calculated in response to 1.5 μL oligomycin (No. 11342, Cayman chemical, MI, USA) injection for 20 minutes. The maximum respiratory capacity was assessed for 30 minutes after the stimulation by 2.5 μM carbonyl cyanide 4-(trifluoromethoxy) phenylhydrazone (FCCP) (Sigma-Aldrich). Finally, mitochondrial respiration was blocked by adding both 2.5 μM rotenone (Sigma) and 1.25 μM antimycin A (Wako), and the residual OCR was considered as nonmitochondrial respiration. Proton leak was calculated by subtracting the nonmitochondrial respiration

components of basal respiration from the ATP turnover rate.

Measurement of citrate synthase activity

Citrate synthase (CS) activity was measured using the BioVision's Citrate Synthase Activity Assay Kit according to the manufacturer's protocol. Cultured brown adipocytes were harvested with 100 μL ice cold CS assay buffer. Supernatants were collected after cells were centrifuged at 10,000 g for 5 minutes. A total of 10 μL sample was used and the volume was adjusted to 50 μL with CS assay buffer. The reaction mix was prepared by mixing 43 μL of CS assay buffer, 5 μL of CS developer, and 2 μL of CS substrate mix for each sample. Immediately after adding 50 μL of the reaction mix to each well, absorbance was measured at OD 412 nm in kinetic mode at 25°C for 40-60 minutes. Citrate synthase activity was calculated by measuring the slope of the graph in the linear range during the reaction time.

Transient transfection and Luciferase reporter assay

COS-7 cells were seeded at 12-well plates the day before transfection. COS-7 cells were transfected with the reporter plasmid UCP1-luciferase (0.3 μg), RSV-βgal (0.1 μg), UBC9 (0.1 μg), pFLAG-SUMO1 (0.1 μg), and the indicated amount of expression vectors of HA-ERRα (0.025 μg), HA-FLAG-PGC1α (0.05 μg), and SENP2 (0.1 μg). The expression vectors were mixed with 2.5 μL of Plus reagent (Invitrogen) in 50 μL of serum free DMEM and were incubated for 15 minutes at room temperature. After additional 15 minutes of incubation upon adding 50 μL of serum free DMEM containing 2.5 μL of Lipofectamine reagent (Invitrogen), the complex was treated to the cells with 400 μL of serum free DMEM. The media was changed to DMEM supplemented with 10% FBS 3 hours later. Cells were harvested 24 hours after transfection using 150 μL of reporter lysis buffer (Promega), and the luciferase activity was determined using 50 μL of the lysates with the Lumat LB 9507 Ultra Sensitive Tube Luminometer

(Berthold, Bad Wildbad, Germany).

Luciferase activity was normalized by β–galactosidase activity. For β–galactosidase activity, 10 μL of lysate was mixed with 3 μL of 100X MgCl2 (0.1M MgCl2, 4.5 M β–mercaptoethanol), 66 μL of 1X O−nitrophenyl−β−D−galactosidase and 201 μL of 0.1 M sodium phosphate (pH 7.5) in a 96 well plate. β–galactosidase activity was measured by spectrophotometry at 420 nm (VersaMax; Molecular devices, Sunnyvale, CA, USA) 25 minutes later.

3. Results

Senp2 knockdown on day 4 does not affect adipogenesis of brown adipocyte

To determine the effect of SENP2 in mature brown adipocytes, mRNA levels of adipogenic transcription factors as well as BAT specific genes were measured during brown preadipocyte differentiation. Gene expression of *Fabp4* increased from day 2 of differentiation and were significant from day 3, serving a role as an adipogenesis marker (Figure 20). The levels of *Ucp1* started to rise from day 3–4 and continued to rise during differentiation.

On siRNA-mediated *Senp2* gene silencing on day 4 of differentiation, the levels of *Fabp4* did not differ compared to the controls (Figure 21A, B). The extent of lipid droplet formation was similar between the groups when examined by light microscope and oil red O staining, suggesting that knockdown of *Senp2* on day 4 did not interfere with adipogenesis (Figure 22).

Genes related to mitochondrial biogenesis, fusion, and fission were not changed by *Senp2* knockdown, and the mtDNA copy number in the siSENP2 treated brown adipocytes was analogous to the controls (Figure 23A, B). Similar staining intensity was seen when labelled with a mitochondrion-selective probe which accumulates in active mitochondria (Figure 24).

I also investigated the mitochondrial function. There was no difference in the extent of citrate synthase enzyme activity between the groups (Figure 25). When cellular oxygen consumption rate was analyzed, the basal OCR and maximal respiration rate were slightly reduced than controls with a trend that approached significance (Figure 26). These results demonstrate that suppressing *Senp2* on day 4 of differentiation does not impair adipogenesis, mitochondrial biogenesis or activity *in vitro*.

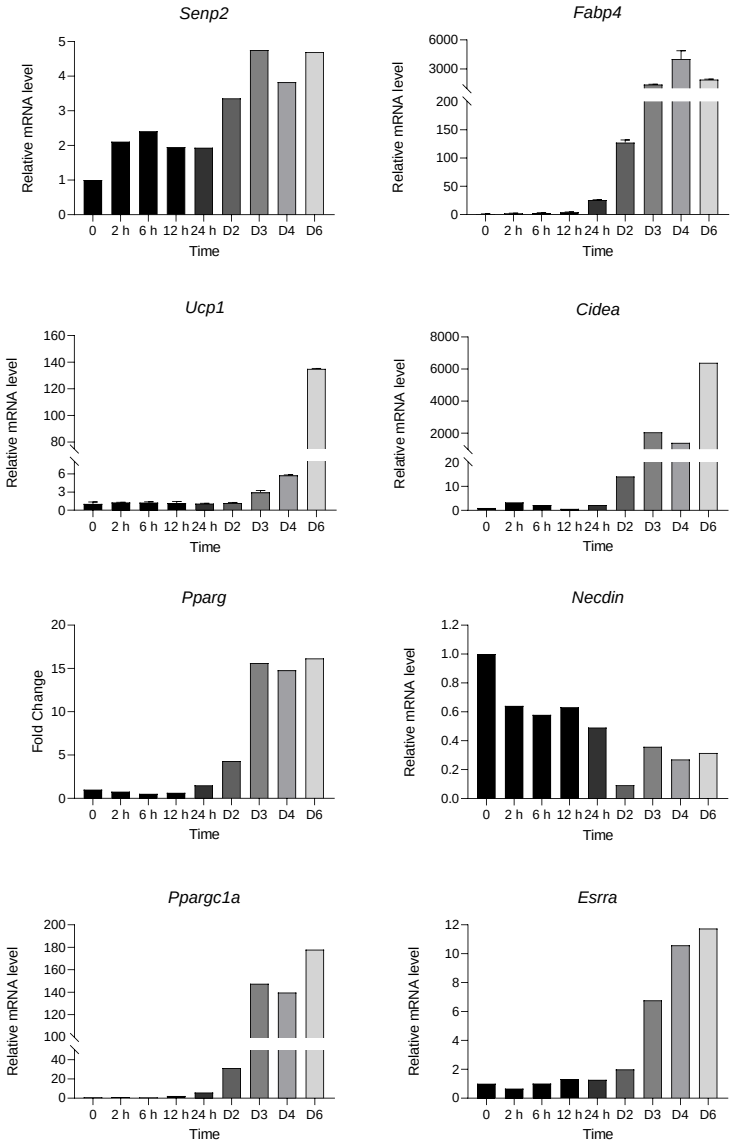

Figure 20. Adipogenic markers rise before the elevation of thermogenic genes during brown adipocyte differentiation

Brown preadipocytes were differentiated according to protocol. *Fabp4* levels started to rise from day 2 of differentiation. Levels of *Ucp1* and *Cidea* were significant from day 3–4 and reached maximum level on day 6. Levels of the mRNA level of each gene in the undifferentiated brown preadipocytes was set to 1.

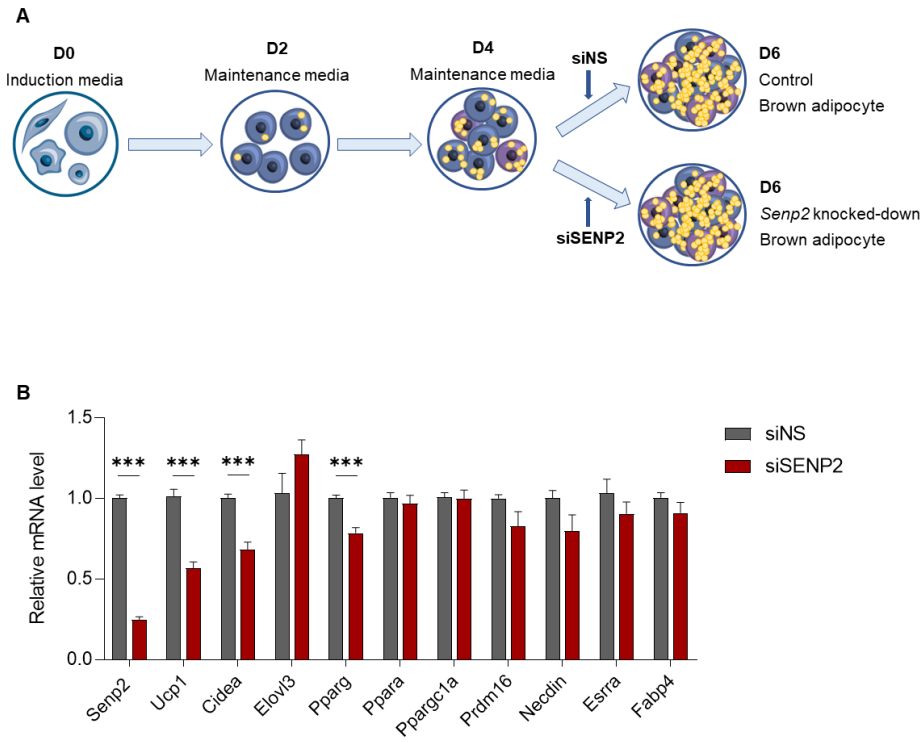

Figure 21. Suppression of *Senp2* results in decreased mRNA levels of thermogenic genes but not adipogenesis

Senp2 was knocked down through reverse transfection during day 4 of differentiation. Cells were harvested two days after. mRNA levels of *Ucp1*, *Cidea*, and *Pparg* decreased upon *Senp2* suppression. *** $P < 0.001$

Fig 21A. Schematic representation of brown adipocyte differentiation and gene knock-down.

Fig 21B. qPCR analysis of genes involved in adipogenesis and thermogenesis upon *Senp2* knock-down. *** $P < 0.001$

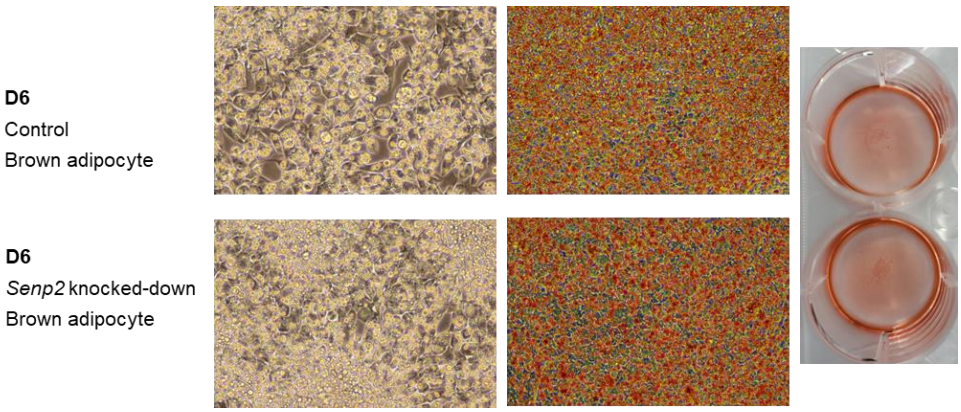

Figure 22. Brown adipocytes transfected with siNS or siSENP2 on day 4 are morphologically similar on examination by light microscope (Left, ×200) or Oil Red O staining (Right, ×100) on day6 of differentiation

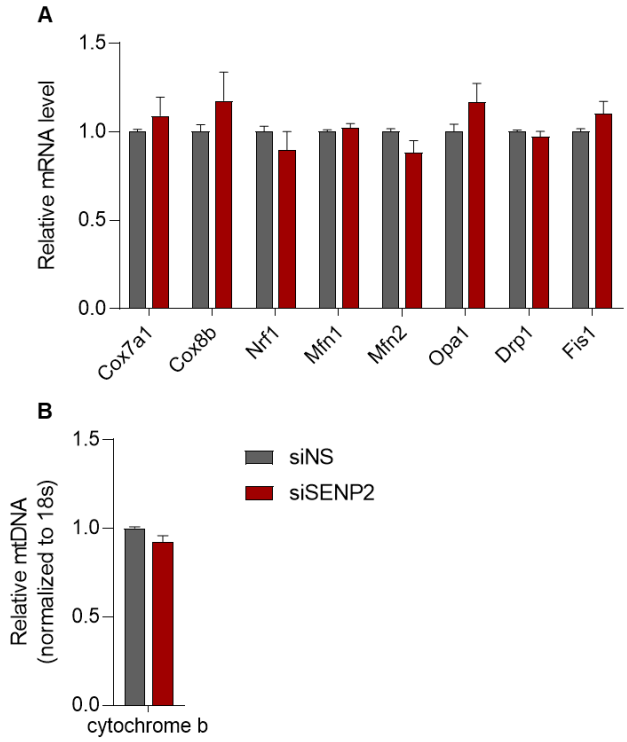

Figure 23. Quantification of genes related to mitochondria in brown adipocytes treated with siNS or siSENP2

Fig 23A. Genes related to mitochondria biogenesis, fusion/fission were unchanged by *Senp2* knockdown

Fig 23B. Similar mtDNA levels in brown adipocytes treated with siNS or siSENP2

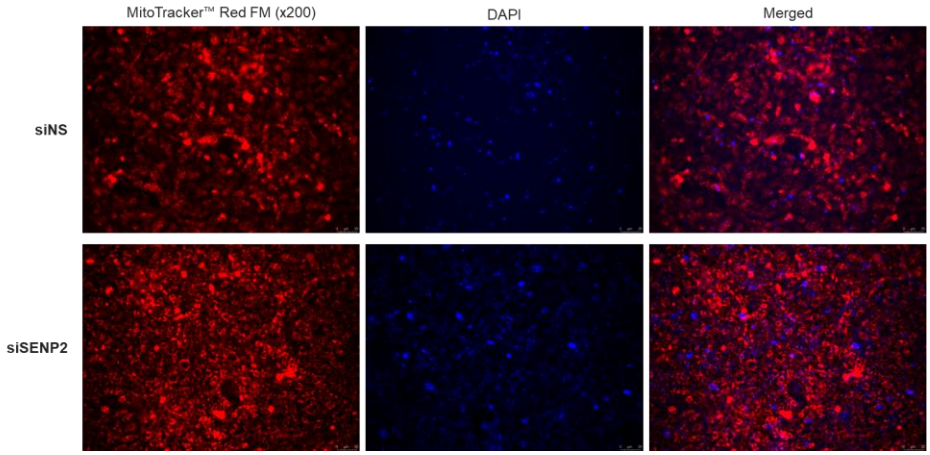

Figure 24. *Senp2* knockdown does not result in change of mitochondrial mass

Brown adipocytes transfected with siNS or siSENP2 were stained with MitoTracker^{tm} Red FM to detect mitochondria. Cell nuclei were counterstained with DAPI. Scale bar = 25 μm.

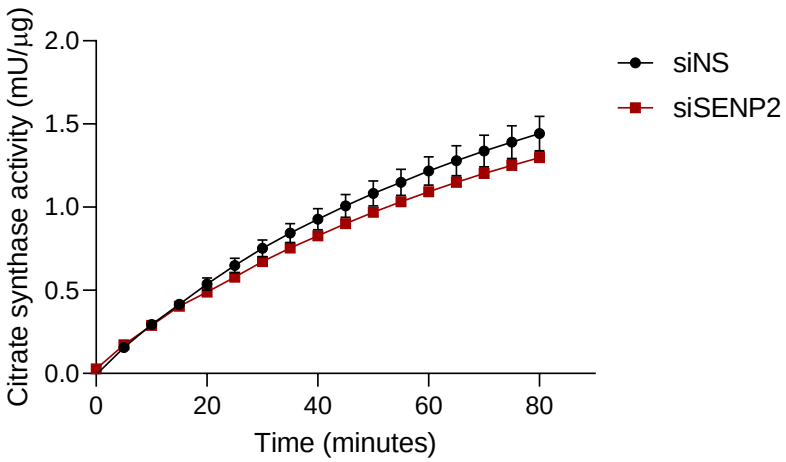

Figure 25. *Senp2* knockdown does not result in change of mitochondrial content

Citrate synthase activity was measured as a surrogate for a quantitative enzyme for the presence of intact mitochondria. Repeated measures ANOVA followed by *post hoc* Tukey's test was used for comparison (P = 0.224 between the groups)

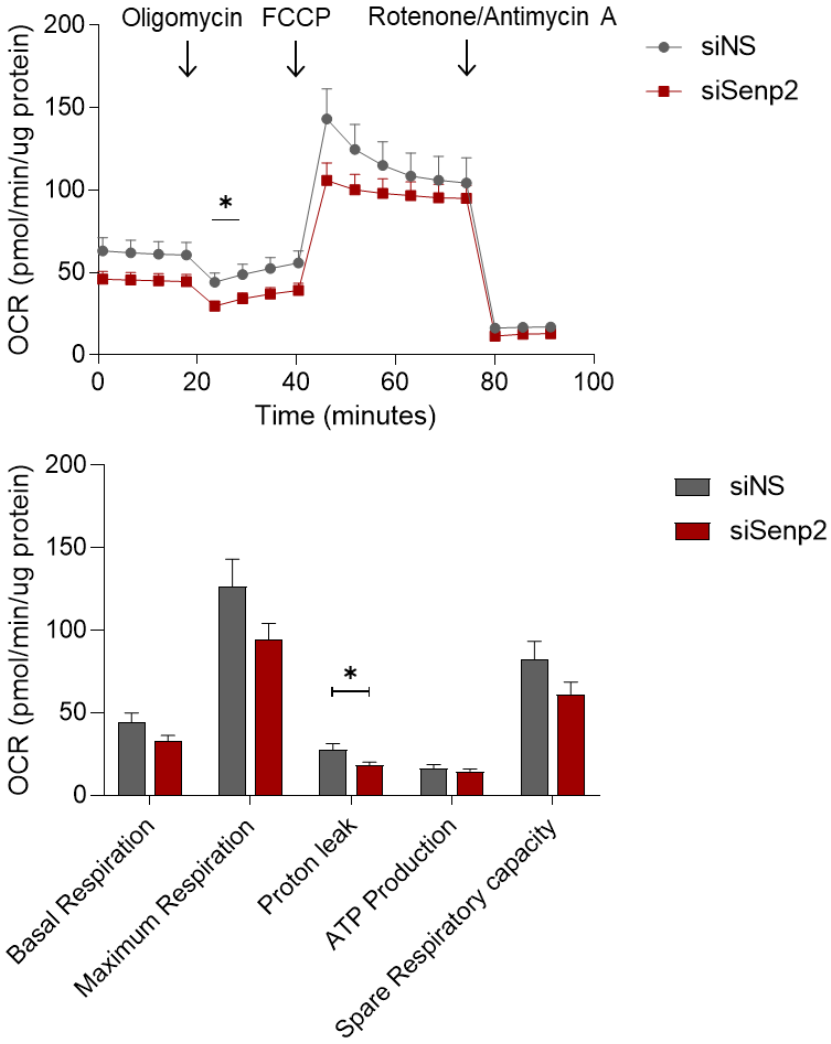

Figure 26. *Senp2* knockdown does not result in change of mitochondrial function

Seahorse assay was performed with brown adipocytes transfected with siNS or siSENP2. Oxygen consumption rates (OCR) values were normalized by total protein amount (μg). n = 10 for each. Representative result from at least three independent experiments. $* P < 0.05$

Ucp1 is downregulated upon SENP2 knockdown

Suppression of *Senp2*, however, resulted in decreased mRNA levels of thermogenic genes. Notably, the levels of *Ucp1* and *Cidea* were consistently downregulated compared to its counterparts at mRNA levels (Figure 21B). *Senp2* knocked-down cells exhibited decreased levels of proton leak under basal conditions, indicative of decreased *Ucp1* levels (Figure 26).

To determine which transcription factor may be associated with the reduction in *Ucp1* levels upon *Senp2* knockdown, siRNAs of *Ppargc1a*, *Esrra*, *Pparg*, and *Ppara* were concurrently transfected with siSENP2 on day 4 of differentiation (Figure 27A, B). Simultaneous knockdown of genes recognized as SUMOylation targets in conjunction with *Senp2* completely abolished the effect of *Senp2* on the expression of *Ucp1* and *Cidea*, with the exception of *Ppara*. Notably, downregulation of *Pparg* markedly reduced the level of *Fabp4*, indicating that *Pparg* knockdown impairs adipogenesis even when transfected on day 4 of differentiation. Knockdown of other genes did not affect adipogenesis. Considering that *Senp2* knockdown reduced the levels of *Ucp1* and *Cidea* without inhibiting adipogenesis, these results collectively suggest that ERRα and PGC-1α may be potential targets in controlling *Ucp1* transcription levels by *Senp2*.

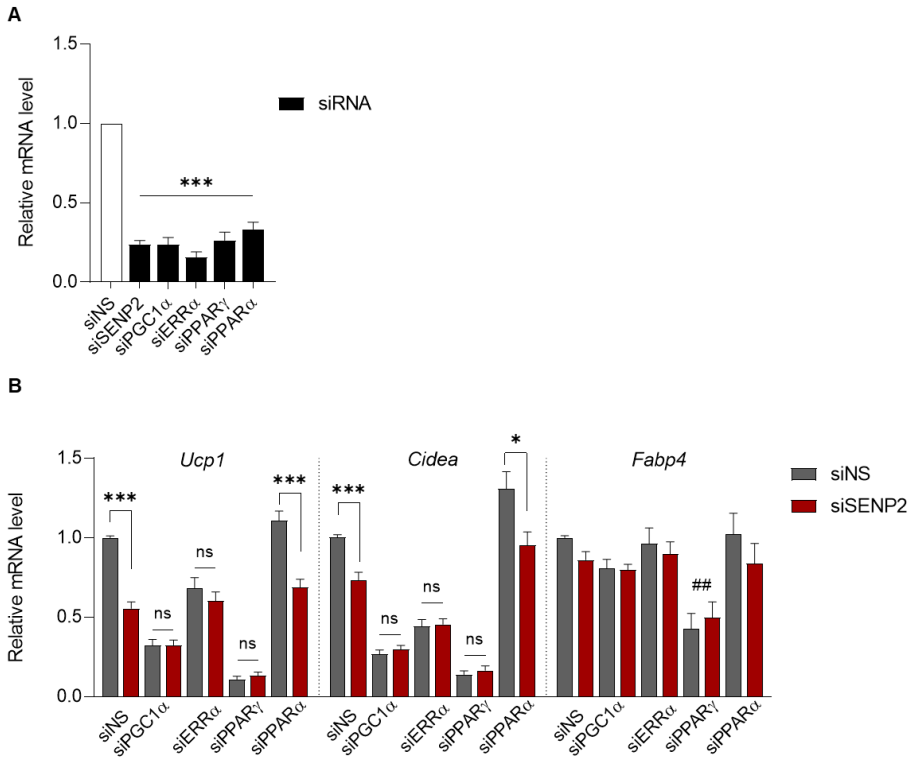

Figure 27. Suppression of *Ppargc1a*, *Esrra*, and *Pparg* abolishes the effect of *Senp2* in *Ucp1* and *Cidea* mRNA levels

Designated siRNAs were treated with siNS or siSENP2 on day 4 of differentiation using reverse transfection method. Cells harvested on day 6 were subjected for qPCR. Total siRNA amount was set to 100 nM. ns, non-significant, * $P < 0.05$, *** $P < 0.001$ by one-way ANOVA and ## $P < 0.01$ by two-way ANOVA followed by Tukey Test

Fig 26A. Effective gene silencing of respective siRNA knockdown

Fig 26B. mRNA levels of *Ucp1*, *Cidea*, and *Fabp4* levels in response to concomitant siRNA knockdown with siSENP2

Transcriptional activation of the Ucp1 gene by ERRα and PGC-1α

To investigate the mechanism by which deSUMOylation enhances *Ucp1* promoter activity, I searched for *cis*-regulatory elements in the *Ucp1* promoter region. *Ucp1* promoter contains a 220-bp enhancer region in the 5-flanking sequence of the *Ucp1* gene that encompasses several *cis*-acting elements of which the sequence is highly conserved between species [53-55].

Within the complex enhancer region 2.5 kb upstream in the *Ucp1* promoter sequence, I identified a PPAR response element (PPRE), and a sequence potentially capable of binding ERRα (Figure 28). The 3.2-kb *Ucp1*-Luc promoter was introduced into COS-7 cells with PPARγ/RXRα and ERRα expression vectors alone or in combination with an expression vector for PGC-1α and luciferase activity was measured. Interestingly, transfection of PPARγ/RXRα, ERRα, and PGC-1α alone induced a modest induction of *Ucp1* gene expression, whereas the combination of ERRα and PGC-1α yielded a marked induction (Figure 29A). *Ucp1* gene expression was increased in proportion to the amount of ERRα and PGC-1α transfected (Figure 29B).

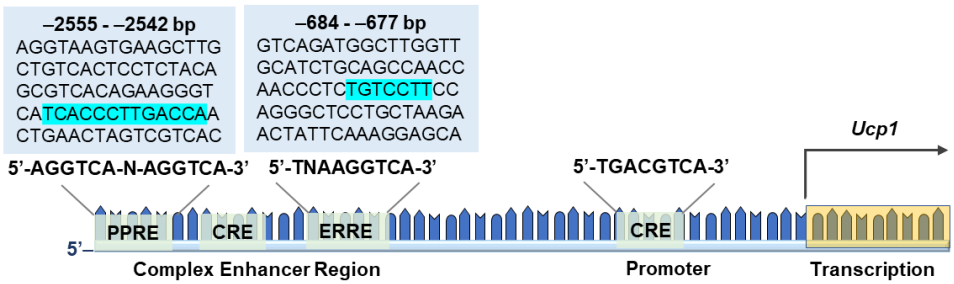

Figure 28. Schematic representation of the *cis*–regulatory regions of *Ucp1* gene

A 3.2–kb *Ucp1*–Luc promoter incorporating both the 220–bp complex enhancer and the proximal promoter region was used for all assays. The complex enhancer region located at 2.5–kb upstream of the transcription start site contains *cis*–acting regulatory sequences that play a critical role in *Ucp1* regulation. These regulatory sequences include PPRE, ERRE, and cAMP responsive elements (CRE).

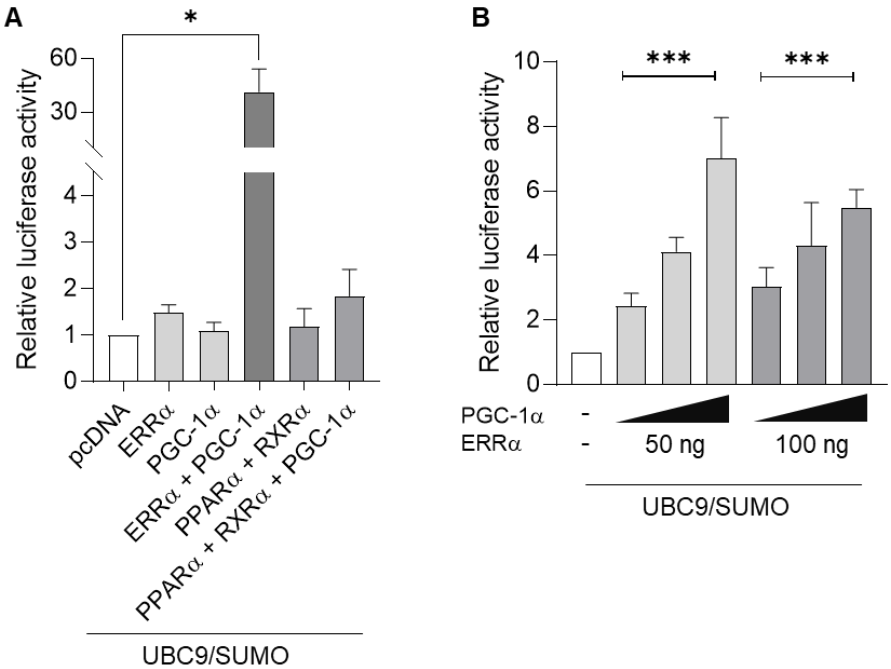

Figure 29. ERRα/PGC−1α transcriptionally activates *Ucp1*

The effect of ERRα, PGC−1α, PPARα/RXRα, alone or in combination with PGC−1α were examined by analyzing the activity of the *Ucp1* reporter gene.

Luciferase activity of the pcDNA transfected cells was set to 1 and others were expressed as their relative values.

Fig 29A. Cotransfection of ERRα (100 ng) and PGC−1α (100 ng) markedly induces *Ucp1* activity

Fig 29B. Transfection of ERRα (50 ng or 100 ng) in combination of PGC−1α (50 ng, 100 ng, or 200 ng) proportionally induces *Ucp1* activity. *** P for trend < 0.001

Senp2 enhances the transcriptional activation of Ucp1 gene

To verify the effect of SUMOylation on the concerted action of ERRα and PGC-1α, an expression vector encoding SUMO fused to the N-terminus of ERRα (SUMO-ERRα) was constructed. Cotransfection of SUMO-ERRα along with the PGC-1α was less effective in increasing the *Ucp1* promoter activity (Figure 30A). On the other hand, overexpression of SENP2 in COS-7 enhanced the *Ucp1* promoter activity upregulated by the cotransfection of ERRα and PGC-1α (Figure 30B). Collectively, these data indicate that deSUMOylation of the ERRα/PGC-1α complex contributes to the increased activity and in turn, *Ucp1* gene expression.

Both ERRα and PGC-1α can be SUMOylated [56, 57]. We have previously verified that the Lys^{14} but not Lys^{402} residue is the major site of SUMOylation for ERRα and that PGC-1α is deSUMOylated only by SENP2 and not by other isoforms of SENP enzymes (Figure 31). To this end, ERRα and PGC-1α expression vectors that contain lysine-to-arginine mutation at the major SUMO conjugation site were generated: ERRα K14R and PGC-1α K183R. Note that transfection of both the wild type and the mutant expression vectors were expressed to similar levels in a concentration-dependent manner (Figure 32). Transfection of wild type ERRα with PGC-1α K183R did not further augment the luciferase activity compared to that from wild type PGC-1α. When ERRα K14R was cotransfected wild type PGC-1α, however, further increase in the luciferase activity was observed (Figure 33). Together, these results suggest that SENP2 regulates the activity of UCP1 promoter through improving the activity of ERRα through deSUMOylation.

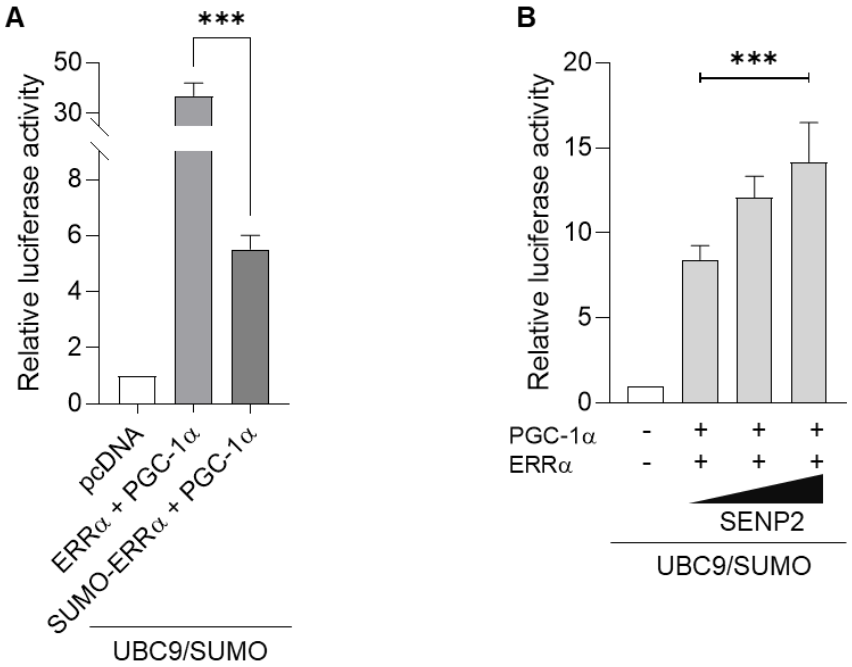

Figure 30. SUMOylation of ERRα/PGC−1α negatively regulates *Ucp1* expression

The effect of ERRα SUMOylation and deSUMOylation by SENP2 were examined by analyzing the activity of the *Ucp1* reporter gene. Luciferase activity of the pcDNA transfected cells was set to 1 and others were expressed as their relative values.

SUMO and UBC9, a SUMO conjugation enzyme, were co−expressed (100 ng, both) to amplify the synergistic effect of ERRα/ PGC−1α.

Fig 30A. Co−transfection of SUMO−ERRα/PGC−1α (25 ng and 50 ng, respectively) resulted in lower luciferase activity level compared to the ERRα/PGC−1α (25 ng and 50 ng, respectively) in wild form (N = 4). *** $P < 0.001$ in Tukey's post hoc analysis in one−way ANOVA

Fig 30B. COS−7 cells were transfected with ERRα/PGC−1α (10 ng and 50 ng, respectively) and increasing amounts of SENP2 expression vector (0, 25, 50 ng) and luciferase activity was measured 24 hours later (N = 5). *** P for trend < 0.001

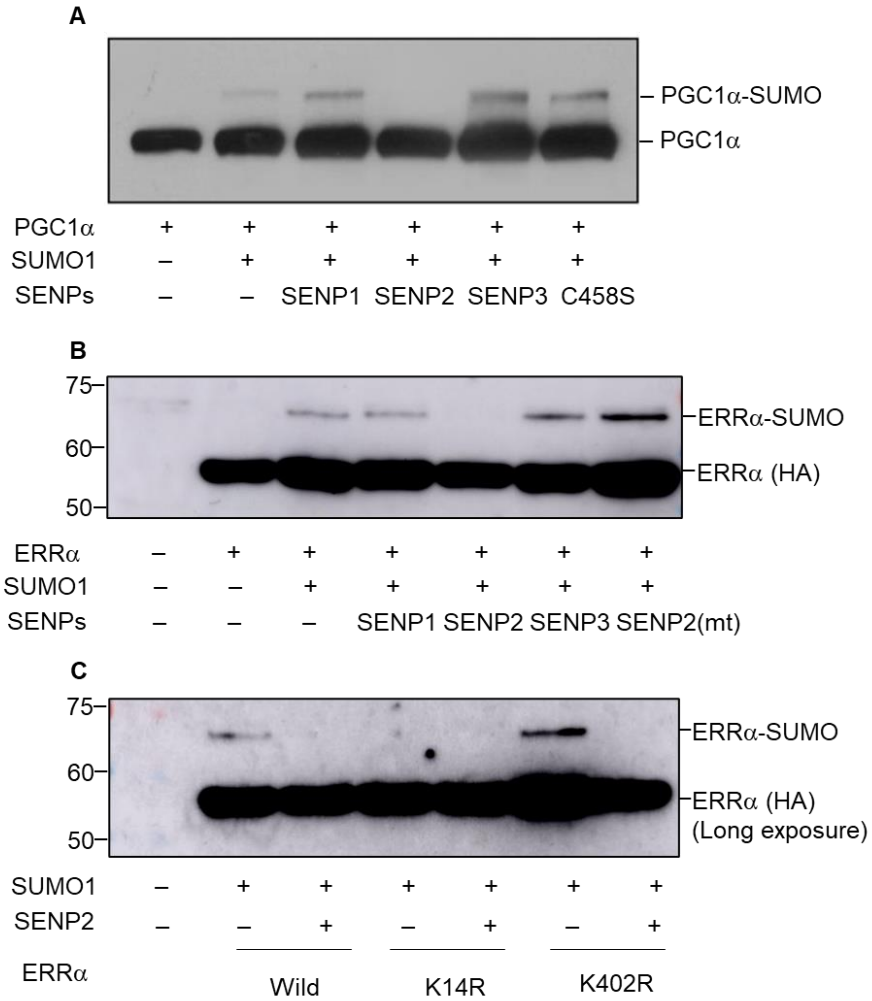

Figure 31. ERRα and PGC-1α are deSUMOylated by SENP2

COS-7 cells transiently transfected with ERRα or PGC-1α with SUMO1 and SENPs (SENP1, SENP2, SENP3, and SENP2 C548S) were harvested 24 hours later and the SUMOylated form was analyzed by immunoblotting.

Fig 31A. PGC-1α can be SUMOylated and is deSUMOylated only by SENP2 (Figure from Jung Eun Min's thesis with permission, 2012)

Fig 31B. ERRα can be SUMOylated and is deSUMOylated only by SENP2

Fig 31C. Lysine 14 is the major SUMOylation site of ERRα and can be deSUMOylated by SENP2

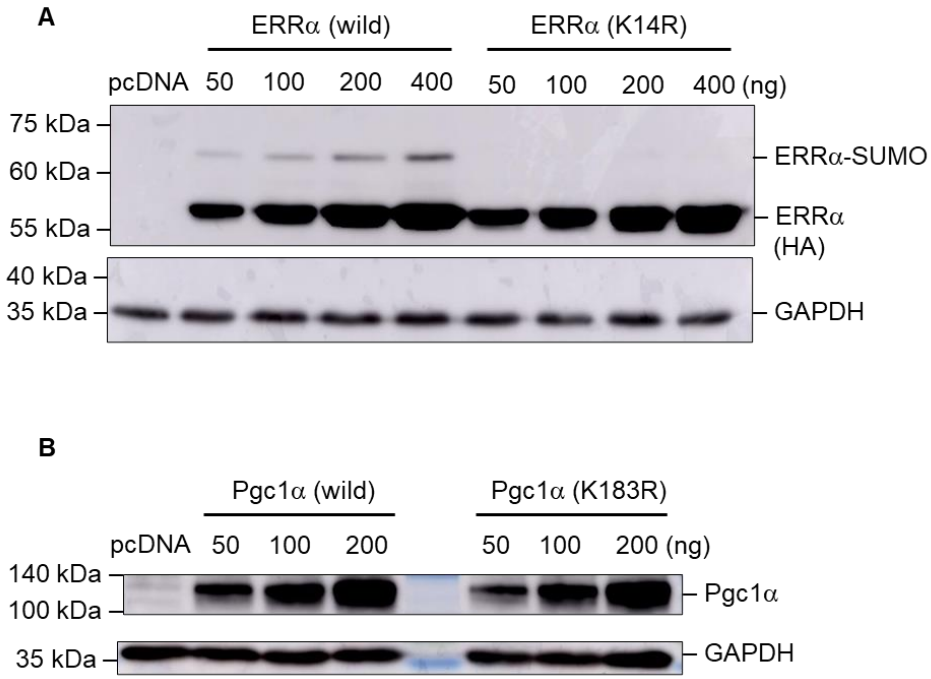

Figure 32. Mutation of SUMOylation site inhibits SUMOylation

COS-7 cells transiently transfected with ERRα, PGC-1α, and their respective mutant expression vectors that contain lysine-to-arginine mutation at the major SUMO conjugation site at increasing concentrations.

SUMO and UBC9 were co-transfected (100 ng, both) to amplify the SUMOylation response.

The cells were harvested 24 hours later and the SUMOylated form was analyzed by immunoblotting.

Fig 32A. SUMO band of wild type ERRα and its absence in the ERRα K14R

Fig 32B. PGC-1α and its mutant form PGC-1α K183R showing same major band intensity at increasing amount of transfection

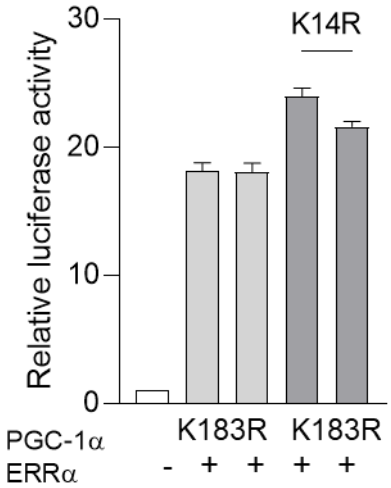

Figure 33. DeSUMOylation of ERRα enhances *Ucp1* activity

COS-7 cells transiently transfected with wild or mutant types of ERRα or PGC-1α. There was no difference in the Ucp1 activity with the PGC-1α wild type or PGC-1α K183R, but the relative luciferase activity increased when ERRα K14R was transfected instead of ERRα wild type.

4. Discussion

We have previously demonstrated that *Cidea* promoter activity is significantly increased by co-transfection of ERRα and PGC-1α (unpublished data). Because ERRα and PGC-1α are intimately associated with *Ucp1* activity and suppressing ERRα or PGC-1α simultaneously with *Senp2* abolished the effect of siSENP2 in additionally decreasing the level of *Ucp1* or *Cidea*, I hypothesized these may be the SUMOylated proteins of which could be accountable for regulating *Ucp1* through SENP2. To this end, transient transfection of expression vectors to COS-7 cells followed by luciferase assay was performed, and I uncovered an analogous mechanism that SENP2 contributed to increasing the UCP1 activity presumably through deSUMOylation of ERRα in the ERRα/PGC-1α complex.

From this mechanistic study, it can be postulated that in the BAT of the *Senp2*-BKO group, SUMOylated form of ERRα/PGC-1α complex was inefficient in augmenting UCP1 upon cold stimuli *in vivo*. Notably, *Ucp1* transcription was increased in proportion to the expression levels of ERRα and PGC-1α. While both ERRα and PGC-1α increased in response to cold stimuli *in vivo*, the extent of increase for both ERRα and PGC-1α was much higher in the *Senp2*$^{f/f}$ group than *Senp2*-BKO.

One possible mechanism involves the activation of CREB. The PGC-1α gene possesses a binding site for CREB (for mice, −146 to −129; in human, −133 to −116) [58]. Increased cAMP levels in response to cold stimuli lead to activation of the CREB by phosphorylation, which in turn enhances the expression of PGC-1α. In a study by Liang et al., deSUMOylation of CREB by SENP2 reduced its interaction with serine/threonine protein phosphatase 2A (PP2A), thereby increasing the level of activated, phosphorylated CREB (pCREB) [17]. In another study by Hatting et al., inhibition of PP2A with okadaic acid effectively rescued pCREB

dephosphorylation to increase CREB-dependent expression of UCP1 [59]. Taken together, these results suggest that SENP2 deSUMOylates CREB to decrease the dephosphorylating action of PP2A, and in turn, enhances the expression of PGC-1α to increase UCP1 upon acute cold exposure.

The *Esrra* promoter contains a multiple steroid hormone response element half-sites (MHRE) (23-bp nucleotides (5-GTGACCTTCATTCGGTCACCGCA-3) and a 11-bp (5-GTGACCTTGAG-3)), which is specifically bound by ERRα [60, 61]. This is a functional ERRE that can act as an autoregulatory element for the synergistic activation of the *Esrra* promoter by binding of the ERRα/PGC-1α complex [61]. Therefore, it can be postulated that deficiency of SENP2 repressed the UCP1 activation in response to cold stimuli by at least two independent mechanisms: SUMOylation of ERRα/PGC-1α complex *per se*, and decreasing the increment of PGC-1α following dephosphorylation of pCREB and in turn downregulating the autoregulatory feed-forward loop.

Unlike in white adipocytes where SENP2 is highly expressed at day 2 of differentiation but are nearly abrogated by day 6 of full differentiation [16], SENP2 is expressed at high levels in brown adipocytes not only in early stages of adipogenesis but also at full maturation. Thereby, while SENP2 is involved in adipogenesis for both white and brown adipocytes, I postulated that there may be a role that SENP2 undertakes regarding BAT function and activity at a later time frame. When *Senp2* was knocked down on day 4 of differentiation, the ability to fully differentiate into mature brown adipocytes was conserved, as with the *Ucp1*-Cre *Senp2*-BKO mice. The levels of *Ucp1* and *Cidea* were downregulated by *Senp2* knockdown, but unstimulated cells were phenotypically similar when mitochondrial function was assessed, in line with the *in vivo* data.

Unfortunately, unlike the *in vivo* model where the characteristics of activated BAT was appreciably better in the *Senp2*$^{f/f}$ control mice in comparison to the *Senp2*-BKO, equivalent response was not simulated by treating the brown adipocytes with adrenergic agents. By treating CL316,243 compound which is a β3-

adrenergic receptor agonist, norepinephrine, or forskolin to increase cAMP levels, both the brown adipocytes transfected with siNS or siSENP2 had *Ucp1* or *Cidea* upregulated to the similar extent, when assessed at different drug concentrations and time points (data not shown). The precise reason for the discrepancy between the *in vivo* and *in vitro* data is obscure. A plausible explanation is that while BAT is a highly innervated tissue, brown adipocytes are denervated and the organ crosstalk is absent in the microenvironment. For instance, in the study by Liu et al., liver-specific SENP2 knockout mice had elevated FGF21 level which in turn increased the O_2 consumption of the BAT [62]. Fully differentiated brown adipocyte cell line was morphologically similar to that from BAT with high expression levels of *Ucp1*, but some of the classical BAT markers such as *Elovl3* and *Dio2* were detected at a very low level in *in vitro* setting. Furthermore, as aforementioned, several other noncanonical pathways of adaptive thermogenesis may be involved that encompasses the effect of SENP2.

With these caveats in mind, I herein report that SENP2 is crucial in maintaining the healthy metabolic phenotype of BAT. ERRα and PGC-1α are pivotal transcriptional regulators that control *Ucp1* and *Cidea* in response to cold or dietary stimuli, and both its activity and expression are influenced by SENP2. Activating BAT is an appealing target to ameliorate metabolic diseases. No approaches to activate BAT directly with pharmacologic agents such as β3 adrenergic receptor agonists or protonophoric compounds, i.e., 2,4-dinitrophenol, have yet been successful with unexpected toxicity. Posttranslational regulation of *Ucp1* through targeting the ERRα/PGC-1α complex by SENP2 may be a potential therapeutic target in combating metabolic derangement caused by metabolic stress.

Bibliography

1. Cannon B, Nedergaard J. Brown adipose tissue: function and physiological significance. Physiol Rev. 2004;84:277-359. doi:10.1152/physrev.00015.2003
2. Kajimura S, Saito M. A new era in brown adipose tissue biology: molecular control of brown fat development and energy homeostasis. Annu Rev Physiol. 2014;76:225-49. doi:10.1146/annurev-physiol-021113-170252
3. Cohade C, Osman M, Pannu HK, Wahl RL. Uptake in supraclavicular area fat ("USA-Fat"): description on 18F-FDG PET/CT. J Nucl Med. 2003;44:170-6.
4. Cypess AM, Lehman S, Williams G, Tal I, Rodman D, Goldfine AB, et al. Identification and importance of brown adipose tissue in adult humans. N Engl J Med. 2009;360:1509-17. doi:10.1056/NEJMoa0810780
5. Orava J, Nuutila P, Lidell ME, Oikonen V, Noponen T, Viljanen T, et al. Different metabolic responses of human brown adipose tissue to activation by cold and insulin. Cell Metab. 2011;14:272-9. doi:10.1016/j.cmet.2011.06.012
6. van Marken Lichtenbelt WD, Vanhommerig JW, Smulders NM, Drossaerts JM, Kemerink GJ, Bouvy ND, et al. Cold-activated brown adipose tissue in healthy men. N Engl J Med. 2009;360:1500-8. doi:10.1056/NEJMoa0808718
7. Virtanen KA, Lidell ME, Orava J, Heglind M, Westergren R, Niemi T, et al. Functional brown adipose tissue in healthy adults. N Engl J Med. 2009;360:1518-25. doi:10.1056/NEJMoa0808949
8. Yoneshiro T, Aita S, Matsushita M, Kameya T, Nakada K, Kawai Y, et al. Brown adipose tissue, whole-body energy expenditure, and thermogenesis in healthy adult men. Obesity (Silver Spring). 2011;19:13-6. doi:10.1038/oby.2010.105
9. Becher T, Palanisamy S, Kramer DJ, Eljalby M, Marx SJ, Wibmer AG, et al. Brown adipose tissue is associated with cardiometabolic health. Nat Med. 2021;27:58-65. doi:10.1038/s41591-020-1126-7
10. Celen AB, Sahin U. Sumoylation on its 25th anniversary: mechanisms, pathology, and emerging concepts. FEBS J. 2020;287:3110-40. doi:10.1111/febs.15319
11. Saitoh H, Hinchey J. Functional heterogeneity of small ubiquitin-related protein modifiers SUMO-1 versus SUMO-2/3. J Biol Chem. 2000;275:6252-8. doi:10.1074/jbc.275.9.6252
12. Geiss-Friedlander R, Melchior F. Concepts in sumoylation: a decade on. Nat Rev Mol Cell Biol. 2007;8:947-56. doi:10.1038/nrm2293
13. Flotho A, Melchior F. Sumoylation: a regulatory protein modification in health and disease. Annu Rev Biochem. 2013;82:357-85. doi:10.1146/annurev-biochem-061909-093311
14. Koo YD, Choi JW, Kim M, Chae S, Ahn BY, Kim M, et al. SUMO-Specific Protease 2 (SENP2) Is an Important Regulator of Fatty Acid

Metabolism in Skeletal Muscle. Diabetes. 2015;64:2420-31. doi:10.2337/db15-0115
15. Nan J, Lee JS, Moon JH, Lee SA, Park YJ, Lee DS, et al. SENP2 regulates mitochondrial function and insulin secretion in pancreatic beta cells. Exp Mol Med. 2022;54:72-80. doi:10.1038/s12276-021-00723-7
16. Chung SS, Ahn BY, Kim M, Choi HH, Park HS, Kang S, et al. Control of adipogenesis by the SUMO-specific protease SENP2. Mol Cell Biol. 2010;30:2135-46. doi:10.1128/MCB.00852-09
17. Liang Q, Zheng Q, Zuo Y, Chen Y, Ma J, Ni P, et al. SENP2 Suppresses Necdin Expression to Promote Brown Adipocyte Differentiation. Cell Rep. 2019;28:2004-11 e4. doi:10.1016/j.celrep.2019.07.083
18. Lee JS, Chae S, Nan J, Koo YD, Lee SA, Park YJ, et al. SENP2 suppresses browning of white adipose tissues by de-conjugating SUMO from C/EBPbeta. Cell Rep. 2022;38:110408. doi:10.1016/j.celrep.2022.110408
19. Gill G. SUMO and ubiquitin in the nucleus: different functions, similar mechanisms? Genes Dev. 2004;18:2046-59. doi:10.1101/gad.1214604
20. Saito M, Matsushita M, Yoneshiro T, Okamatsu-Ogura Y. Brown Adipose Tissue, Diet-Induced Thermogenesis, and Thermogenic Food Ingredients: From Mice to Men. Front Endocrinol (Lausanne). 2020;11:222. doi:10.3389/fendo.2020.00222
21. Inokuma K, Ogura-Okamatsu Y, Toda C, Kimura K, Yamashita H, Saito M. Uncoupling protein 1 is necessary for norepinephrine-induced glucose utilization in brown adipose tissue. Diabetes. 2005;54:1385-91. doi:10.2337/diabetes.54.5.1385
22. Shan T, Liang X, Bi P, Zhang P, Liu W, Kuang S. Distinct populations of adipogenic and myogenic Myf5-lineage progenitors in white adipose tissues. J Lipid Res. 2013;54:2214-24. doi:10.1194/jlr.M038711
23. Song A, Dai W, Jang MJ, Medrano L, Li Z, Zhao H, et al. Low- and high-thermogenic brown adipocyte subpopulations coexist in murine adipose tissue. J Clin Invest. 2020;130:247-57. doi:10.1172/JCI129167
24. Houstek J, Kopecky J, Rychter Z, Soukup T. Uncoupling protein in embryonic brown adipose tissue--existence of nonthermogenic and thermogenic mitochondria. Biochim Biophys Acta. 1988;935:19-25. doi:10.1016/0005-2728(88)90103-x
25. Golozoubova V, Cannon B, Nedergaard J. UCP1 is essential for adaptive adrenergic nonshivering thermogenesis. Am J Physiol Endocrinol Metab. 2006;291:E350-7. doi:10.1152/ajpendo.00387.2005
26. Ikeda K, Kang Q, Yoneshiro T, Camporez JP, Maki H, Homma M, et al. UCP1-independent signaling involving SERCA2b-mediated calcium cycling regulates beige fat thermogenesis and systemic glucose homeostasis. Nat Med. 2017;23:1454-65. doi:10.1038/nm.4429
27. Ikeda K, Yamada T. UCP1 Dependent and Independent Thermogenesis in Brown and Beige Adipocytes. Front Endocrinol (Lausanne). 2020;11:498. doi:10.3389/fendo.2020.00498
28. Chouchani ET, Kazak L, Spiegelman BM. New Advances in Adaptive Thermogenesis: UCP1 and Beyond. Cell Metab. 2019;29:27-37.

doi:10.1016/j.cmet.2018.11.002
29. Kazak L, Chouchani ET, Jedrychowski MP, Erickson BK, Shinoda K, Cohen P, et al. A creatine-driven substrate cycle enhances energy expenditure and thermogenesis in beige fat. Cell. 2015;163:643-55. doi:10.1016/j.cell.2015.09.035
30. Villarroya J, Cereijo R, Gavalda-Navarro A, Peyrou M, Giralt M, Villarroya F. New insights into the secretory functions of brown adipose tissue. J Endocrinol. 2019;243:R19-R27. doi:10.1530/JOE-19-0295
31. Chartoumpekis DV, Habeos IG, Ziros PG, Psyrogiannis AI, Kyriazopoulou VE, Papavassiliou AG. Brown adipose tissue responds to cold and adrenergic stimulation by induction of FGF21. Mol Med. 2011;17:736-40. doi:10.2119/molmed.2011.00075
32. Hondares E, Iglesias R, Giralt A, Gonzalez FJ, Giralt M, Mampel T, et al. Thermogenic activation induces FGF21 expression and release in brown adipose tissue. J Biol Chem. 2011;286:12983-90. doi:10.1074/jbc.M110.215889
33. Hanssen MJ, Broeders E, Samms RJ, Vosselman MJ, van der Lans AA, Cheng CC, et al. Serum FGF21 levels are associated with brown adipose tissue activity in humans. Sci Rep. 2015;5:10275. doi:10.1038/srep10275
34. Wang GX, Zhao XY, Meng ZX, Kern M, Dietrich A, Chen Z, et al. The brown fat-enriched secreted factor Nrg4 preserves metabolic homeostasis through attenuation of hepatic lipogenesis. Nat Med. 2014;20:1436-43. doi:10.1038/nm.3713
35. Cao W, Daniel KW, Robidoux J, Puigserver P, Medvedev AV, Bai X, et al. p38 mitogen-activated protein kinase is the central regulator of cyclic AMP-dependent transcription of the brown fat uncoupling protein 1 gene. Mol Cell Biol. 2004;24:3057-67. doi:10.1128/MCB.24.7.3057-3067.2004
36. Finck BN, Kelly DP. PGC-1 coactivators: inducible regulators of energy metabolism in health and disease. J Clin Invest. 2006;116:615-22. doi:10.1172/JCI27794
37. LeBleu VS, O'Connell JT, Gonzalez Herrera KN, Wikman H, Pantel K, Haigis MC, et al. PGC-1alpha mediates mitochondrial biogenesis and oxidative phosphorylation in cancer cells to promote metastasis. Nat Cell Biol. 2014;16:992-1003, 1-15. doi:10.1038/ncb3039
38. Puigserver P, Wu Z, Park CW, Graves R, Wright M, Spiegelman BM. A cold-inducible coactivator of nuclear receptors linked to adaptive thermogenesis. Cell. 1998;92:829-39. doi:10.1016/s0092-8674(00)81410-5
39. Wu Z, Puigserver P, Andersson U, Zhang C, Adelmant G, Mootha V, et al. Mechanisms controlling mitochondrial biogenesis and respiration through the thermogenic coactivator PGC-1. Cell. 1999;98:115-24. doi:10.1016/S0092-8674(00)80611-X
40. Schreiber SN, Knutti D, Brogli K, Uhlmann T, Kralli A. The transcriptional coactivator PGC-1 regulates the expression and activity of the orphan nuclear receptor estrogen-related receptor alpha (ERRalpha). J Biol Chem. 2003;278:9013-8. doi:10.1074/jbc.M212923200
41. Huss JM, Kopp RP, Kelly DP. Peroxisome proliferator-activated receptor coactivator-1alpha (PGC-1alpha) coactivates the cardiac-enriched

nuclear receptors estrogen-related receptor-alpha and -gamma. Identification of novel leucine-rich interaction motif within PGC-1alpha. J Biol Chem. 2002;277:40265-74. doi:10.1074/jbc.M206324200
42. Lin J, Yang R, Tarr PT, Wu PH, Handschin C, Li S, et al. Hyperlipidemic effects of dietary saturated fats mediated through PGC-1beta coactivation of SREBP. Cell. 2005;120:261-73. doi:10.1016/j.cell.2004.11.043
43. Vega RB, Huss JM, Kelly DP. The coactivator PGC-1 cooperates with peroxisome proliferator-activated receptor alpha in transcriptional control of nuclear genes encoding mitochondrial fatty acid oxidation enzymes. Mol Cell Biol. 2000;20:1868-76. doi:10.1128/MCB.20.5.1868-1876.2000
44. Puigserver P, Spiegelman BM. Peroxisome proliferator-activated receptor-gamma coactivator 1 alpha (PGC-1 alpha): transcriptional coactivator and metabolic regulator. Endocr Rev. 2003;24:78-90. doi:10.1210/er.2002-0012
45. Knutti D, Kralli A. PGC-1, a versatile coactivator. Trends Endocrinol Metab. 2001;12:360-5. doi:10.1016/s1043-2760(01)00457-x
46. Brown EL, Hazen BC, Eury E, Wattez JS, Gantner ML, Albert V, et al. Estrogen-Related Receptors Mediate the Adaptive Response of Brown Adipose Tissue to Adrenergic Stimulation. iScience. 2018;2:221-37. doi:10.1016/j.isci.2018.03.005
47. Gantner ML, Hazen BC, Eury E, Brown EL, Kralli A. Complementary Roles of Estrogen-Related Receptors in Brown Adipocyte Thermogenic Function. Endocrinology. 2016;157:4770-81. doi:10.1210/en.2016-1767
48. Schreiber SN, Emter R, Hock MB, Knutti D, Cardenas J, Podvinec M, et al. The estrogen-related receptor alpha (ERRalpha) functions in PPARgamma coactivator 1alpha (PGC-1alpha)-induced mitochondrial biogenesis. Proc Natl Acad Sci U S A. 2004;101:6472-7. doi:10.1073/pnas.0308686101
49. Giralt A, Hondares E, Villena JA, Ribas F, Diaz-Delfin J, Giralt M, et al. Peroxisome proliferator-activated receptor-gamma coactivator-1alpha controls transcription of the Sirt3 gene, an essential component of the thermogenic brown adipocyte phenotype. J Biol Chem. 2011;286:16958-66. doi:10.1074/jbc.M110.202390
50. Kong X, Wang R, Xue Y, Liu X, Zhang H, Chen Y, et al. Sirtuin 3, a new target of PGC-1alpha, plays an important role in the suppression of ROS and mitochondrial biogenesis. PLoS One. 2010;5:e11707. doi:10.1371/journal.pone.0011707
51. Debevec D, Christian M, Morganstein D, Seth A, Herzog B, Parker M, et al. Receptor interacting protein 140 regulates expression of uncoupling protein 1 in adipocytes through specific peroxisome proliferator activated receptor isoforms and estrogen-related receptor alpha. Mol Endocrinol. 2007;21:1581-92. doi:10.1210/me.2007-0103
52. Ahmadian M, Liu S, Reilly SM, Hah N, Fan W, Yoshihara E, et al. ERRgamma Preserves Brown Fat Innate Thermogenic Activity. Cell Rep. 2018;22:2849-59. doi:10.1016/j.celrep.2018.02.061
53. Kozak UC, Kopecky J, Teisinger J, Enerback S, Boyer B, Kozak LP.

An upstream enhancer regulating brown-fat-specific expression of the mitochondrial uncoupling protein gene. Mol Cell Biol. 1994;14:59-67. doi:10.1128/mcb.14.1.59-67.1994
54. Cassard-Doulcier AM, Gelly C, Fox N, Schrementi J, Raimbault S, Klaus S, et al. Tissue-specific and beta-adrenergic regulation of the mitochondrial uncoupling protein gene: control by cis-acting elements in the 5'-flanking region. Mol Endocrinol. 1993;7:497-506. doi:10.1210/mend.7.4.8388995
55. Sears IB, MacGinnitie MA, Kovacs LG, Graves RA. Differentiation-dependent expression of the brown adipocyte uncoupling protein gene: regulation by peroxisome proliferator-activated receptor gamma. Mol Cell Biol. 1996;16:3410-9. doi:10.1128/MCB.16.7.3410
56. Rytinki MM, Palvimo JJ. SUMOylation attenuates the function of PGC-1alpha. J Biol Chem. 2009;284:26184-93. doi:10.1074/jbc.M109.038943
57. Hietakangas V, Anckar J, Blomster HA, Fujimoto M, Palvimo JJ, Nakai A, et al. PDSM, a motif for phosphorylation-dependent SUMO modification. Proc Natl Acad Sci U S A. 2006;103:45-50. doi:10.1073/pnas.0503698102
58. Fernandez-Marcos PJ, Auwerx J. Regulation of PGC-1alpha, a nodal regulator of mitochondrial biogenesis. Am J Clin Nutr. 2011;93:884S-90. doi:10.3945/ajcn.110.001917
59. Hatting M, Rines AK, Luo C, Tabata M, Sharabi K, Hall JA, et al. Adipose Tissue CLK2 Promotes Energy Expenditure during High-Fat Diet Intermittent Fasting. Cell Metab. 2017;25:428-37. doi:10.1016/j.cmet.2016.12.007
60. Liu D, Zhang Z, Gladwell W, Teng CT. Estrogen stimulates estrogen-related receptor alpha gene expression through conserved hormone response elements. Endocrinology. 2003;144:4894-904. doi:10.1210/en.2003-0432
61. Laganiere J, Tremblay GB, Dufour CR, Giroux S, Rousseau F, Giguere V. A polymorphic autoregulatory hormone response element in the human estrogen-related receptor alpha (ERRalpha) promoter dictates peroxisome proliferator-activated receptor gamma coactivator-1alpha control of ERRalpha expression. J Biol Chem. 2004;279:18504-10. doi:10.1074/jbc.M313543200
62. Liu Y, Dou X, Zhou WY, Ding M, Liu L, Du RQ, et al. Hepatic Small Ubiquitin-Related Modifier (SUMO)-Specific Protease 2 Controls Systemic Metabolism Through SUMOylation-Dependent Regulation of Liver-Adipose Tissue Crosstalk. Hepatology. 2021;74:1864-83. doi:10.1002/hep.31881

국문 초록

갈색지방조직은 최근 대사적으로 주목받고 있는 내분비 기관이다. 갈색지방조직은 기존에 잘 알려진 비오한 열생산을 통한 체온 유지 외에도, 에너지 소모량을 증가시키고 여분의 에너지가 체내에 축적되는 것을 막아주는 등 대사적으로 좋은 역할을 하는 것으로 밝혀졌다. 최근 성인에서도 갈색지방조직의 존재가 확인됨에 따라, 갈색지방조직을 활성화시키기 위한 다양한 노력이 시도되고 있다. SENP2는 단백질 번역 후 변형에 관여하는 효소로 구체적으로는 SUMO를 제거해줌으로써 다양한 단백질의 활성 정도를 조절한다. SENP2가 기관에 따라 대사적으로 중요한 역할을 하는 것은 기존 연구를 통하여 많이 밝혀왔으나, 갈색지방조직에서의 대사적 역할에 대한 연구는 미비한 실정이다.

본 연구에서 *Ucp1*-Cre를 이용하여 갈색지방조직 특이적으로 *Senp2* 유전자를 제거하였으며(*Senp2*-BKO), 정상 대조군과($Senp2^{f/f}$) 비교하여 그 표현형을 관찰하였다. *Senp2*-BKO 마우스는 $Senp2^{f/f}$ 마우스와 비교하였을 때, 상온에서 일반 식이를 진행하였을 때 체중이나 혈당 등 대사적인 지표에서 차이를 보이지 않았으나, 고지방 함유식을 13주 이상 섭취할 경우 체중이나 지방량의 차이를 보이기 전에 인슐린 저항성이 나빠지는 결과를 보였다. 또한 일반 식이를 진행한 마우스에서도, 저온 노출 실험 진행 시 3시간 이후부터는 *Senp2*-BKO 마우스에서 비오한 열생산이 효율적으로 작용하지 못하여 중심부 체온 유지가 잘 되지 않는 점을 반복적으로 확인하였다.

저온 노출 실험을 진행한 쥐의 갈색지방조직 유전자 발현을 확인하였을 때, 대조군 마우스에서는 *Ucp1*, *Cidea*와 같은 열생산에 관여하는 유전자가 큰 폭으로 증가하였으나, *Senp2*-BKO 마우스의 경우 해당 유전자가 상온에서의 발현 정도 대비 적은 폭으로 증가하였기에, 이를 통해 SENP2가 갈색지방조직의 활성화에 기여한다는 점을 추론할 수 있었다.

분자생물학적인 기전을 확인하기 위하여 갈색지방세포주를 분화시켜

분화 단계 별 유전자 발현을 확인하였다. 갈색지방조직의 분화 마커로 사용되는 *Fabp4*의 경우 분화 2일차부터 증가하여 3-4일 차에는 분화가 완료된 세포에서와 비슷한 정도의 발현을 보였으나, *Ucp1*과 *Cidea*의 경우 분화 4일 차부터 증가하여 6일차에 발현이 최대치가 되었다. 이에 갈색지방세포 분화 4일차에 siRNA를 이용하여 유전자 발현을 저해하였으며, 분화 6일차에 유전자 발현을 확인한 결과 siSENP2를 처리한 세포에서 대조군 세포 대비 *Fabp4* 유전자 발현 정도는 같으며 *Ucp1*과 *Cidea*가 감소하는 것을 확인하였다. 이를 통해, 갈색지방세포 분화 4일차에 siRNA를 이용하여 *Senp2* 발현을 억제할 시 *Ucp1*-Cre를 이용한 동물 모델에서와 마찬가지로 갈색지방조직의 분화에는 영향을 미치지 않으면서 열생산과 관련된 유전자의 발현 정도를 저해한다는 점을 확인할 수 있었다.

본 실험실에서는 기존에 SENP2가 ERRα와 PGC-1α를 통해 *Cidea*의 발현을 조절할 수 있다는 점을 확인한 바 있다. 금번 연구를 통해 *Ucp1* 프로모터 영역에도 ERRα이 결합할 수 있는 부위가 있는 것을 확인하였으며, COS-7 세포를 이용한 transient transfection 및 luciferase assay를 통하여, 마찬가지로 ERRα이 PGC-1α과 함께 결합하였을 때 *Ucp1* 활성이 극대화되는 것을 확인하였다. ERRα 전사인자에 SUMO를 결합시킬 경우 *Ucp1*을 활성화시키는 정도가 감소하였으며, 반대로 ERRα/PGC-1α 복합체에 SENP2를 넣어줄 경우 농도 의존적으로 *Ucp1* 활성이 증가됨을 알 수 있었다. ERRα에서 SUMO가 붙고 SENP2에 의해 작용하는 Lysine 14번과, PGC-1α에서 SENP2의 작용 위치로 알려진 Lysine 183번을 각각 Arginine으로 치환하였을 때, PGC-1α 돌연변이에 의해서는 *Ucp1* 활성이 유의미하게 변화하지 않았으나, ERRα 돌연변이에 의해서는 *Ucp1* 활성이 소폭 증가하는 것이 확인되었다. 이를 통해 SENP2가 ERRα의 Lysine 14번 자리를 탈수모화시키는 것이, 갈색지방조직에서 *Ucp1* 활성을 높게 유지하는데 중요한 기전임을 알 수 있었다. 추가적인 기전에 연구는 현재 진행 중이다.

이를 통해 SENP2는 갈색 지방 조직에서 대사적인 활성을 조절하는

중요한 효소임을 밝혀내었으며, 실험을 통해 그 기전을 일부 증명하였다. 추후 SENP2가 대사 질환의 치료에 있어서 갈색 지방 조직을 활성화시키는데 중요한 후보 물질로 활용되기를 기대하는 바이다.

감사의 글

박사 학위 과정은 저에게 있어서 과학자로 성장할 수 있었던 소중한 기간이었습니다. 지면을 빌어 그 과정에서 도움을 주신 많은 분들에게 감사의 말씀을 드립니다.

내분비대사내과 의사로, 또 연구를 처음 시작하는 대학원 학생으로서 발걸음을 내딛을 수 있게 지도해주신 박경수 교수님께 감사드립니다. 첫 면담 때, 의학박사란 자립적으로 실험을 할 수 있는 과학자로서 독립하여 의학계 발전에 기여하는 연구를 수행한다는 의미를 지닌다고 하신 말씀이 기억에 남습니다. 앞으로도 이를 되새기며, 의학박사로서 끊임없이 발전해 나가는 모습으로 가르침에 보답하겠습니다.

실험을 계획하고 수행하는 모든 과정을 세심하게 가르쳐 주시고 물심양면으로 도와주신 정성수 박사님과 이승아 박사님께 감사 인사를 드리고 싶습니다. 실험이 계획대로 잘 나오지 않을 때도, 차근차근 해 나가다 보면 새로운 사실도 알고 재미있는 현상도 찾을 수 있으므로 조금은 느긋하고 담대하게 진행하자고 조언해주신 것이 큰 힘이 되었습니다.

학위 과정 동안, 데이터를 상의하고 문제 해결 방안을 함께 모색하며 크고 작은 부분에서 도움을 준 많은 선생님들에게 고마운 마음을 전합니다. 양원모 박사님, 이지선 박사님, 박종연 선생님, 김성균 선생님, 남금연 선생님, 김수빈 선생님, 윤예슬 선생님을 비롯한 실험실 연구원들 덕분에 본 실험을 잘 진행할 수 있었습니다. 함께 보낸 시간이 값지고 따뜻하고 의미있었습니다. 함께하지는 않았으나, 과거 학위 논문을 통해 저에게 실험 방향에 대한 영감을 준 민정은 선생님도 감사합니다.

학위 논문을 심사하는 과정에서 연말 귀중한 시간을 내어 건설적인 조언을 해주신 김종일 교수님, 조영민 교수님, 이혁준 교수님, 그리고 김하일 교수님께 감사드립니다.

저에게는 너무나 큰 의미가 있는 연구였고, 보람찬 학위 과정이었습니다. 본 연구를 시작으로 앞으로도 훌륭한 의학 박사로 정진하고 의학계에 기여할 수 있도록 노력하겠습니다.